PRR14 organizes H3K9me3-modifed heterochromatin at the nuclear lamina.

Anna A. Kiseleva[1], Yu-Chia Cheng[1], Cheryl L. Smith[1], Richard A. Katz[2], and Andrey Poleshko[1]*

[1] Department of Cell and Developmental Biology, Perelman School of Medicine, University of Pennsylvania, Philadelphia, Pennsylvania, USA.

[2] Institute for Cancer Research, Fox Chase Cancer Center, Philadelphia, Pennsylvania, USA.

* Corresponding author.

Correspondence:

Andrey Poleshko
SCTR 09-188
3400 Civic Center Blvd.
Philadelphia, PA 19104
+1 (215) 898-0252
poleshko@pennmedicine.upenn.edu

ABSTRACT

The eukaryotic genome is organized in three dimensions within the nucleus. Transcriptionally active chromatin is spatially separated from silent heterochromatin, a large fraction of which is located at the nuclear periphery. However, the mechanisms by which chromatin is localized at the nuclear periphery remain poorly understood. Here we demonstrate that Proline Rich 14 (PRR14) protein specifically organizes H3K9me3-modified heterochromatin at the nuclear lamina. We show that PRR14 dynamically associates with both the nuclear lamina and heterochromatin, and is able to reorganize heterochromatin in the nucleus of interphase cells independent of mitosis. We demonstrate that PRR14 can bind all isoforms of heterochromatin protein 1 (HP1). We characterize two functional HP1-binding sites within PRR14 that contribute to its association with heterochromatin. Results of fluorescent recovery after photobleaching (FRAP) and super-resolution imaging, indicate that PPR14 forms an anchoring surface for heterochromatin at the nuclear lamina where it interacts dynamically with HP1-associated, H3K9me3-modified chromatin. Our study reveals the mechanism through which PRR14 tethers heterochromatin to the nuclear lamina and we propose a model of dynamic heterochromatin organization at the nuclear periphery.

59 **INTRODUCTION**

60 The eukaryotic genome is organized at multiple scales in the nucleus. The genome is spatially arranged
61 in subnuclear compartments so that transcriptionally active euchromatin is spatially segregated from
62 silent heterochromatin (*1-4*). One example of spatially organized chromatin is transcriptionally silent
63 heterochromatin sequestered at the periphery of the nucleus (*5, 6*). This precise organization of
64 heterochromatin at the nuclear periphery contributes to many cellular functions such as mechanical
65 force response, cell migration, signaling, transparency to light, and transcription control (reviewed in
66 (*1-4, 7, 8*)). Multiple studies have shown that chromatin localization in the nucleus is often correlated
67 with its transcriptional state: more often active when located in the nuclear interior and more often
68 silenced when sequestered to the nuclear periphery (*9-11*). During development and lineage
69 commitment, chromatin in the nucleus undergoes notable spatial reorganization with lineage-specific
70 genes moving towards the nuclear interior while genes that are no longer required move to the nuclear
71 lamina and become transcriptionally silenced (*5*). It has been demonstrated that correct spatial
72 organization of heterochromatin at the nuclear lamina is essential for cell differentiation and lineage
73 maintenance (*12-14*), however we know surprisingly little about the cellular mechanisms (epigenetic
74 modifications, protein complexes, signaling pathways etc.) that orchestrate three-dimensional
75 chromatin positioning within the nucleus in mammalian cells.

76 To date, only a few proteins have been shown to tether chromatin to the nuclear periphery (*15*). Lamin
77 B Receptor (LBR) has been identified as an inner nuclear membrane protein that binds
78 heterochromatin through the adapter protein Heterochromatin Protein 1 (HP1) (*16, 17*). Later studies
79 identified the *C. elegans* CEC-4 protein as a membrane-associated heterochromatin tether (*13*) and
80 mammalian Proline Rich 14 protein (PRR14) as a nuclear lamina-binding protein that also binds
81 heterochromatin through the HP1 adapter (*18*). While mammalian LBR and PRR14 proteins bind
82 heterochromatin through HP1, CEC-4 itself encodes an HP1-like domain (*13*), thereby obviating the
83 need for an HP1 adapter. It is notable that all of the known peripheral heterochromatin tethers utilize
84 a similar mechanism for heterochromatin binding.

85 Mammalian cells utilize three isoforms of HP1– HP1α, HP1β and HP1γ – which vary in their function
86 and localization in the nucleus (*19-22*). HP1α and β isoforms are largely found in association with
87 heterochromatin (*23*), while HP1γ is found in both heterochromatin and euchromatin compartments
88 throughout the nucleus (*24, 25*). All HP1 isoforms are known to bind methylated Lys9 residue on
89 Histone H3 tail (H3K9me) (*26, 27*). Both H3K9me2 and H3K9me3 histone modifications have been
90 associated with heterochromatin, but specificity of interacting proteins has not been well defined.

91 LBR and CEC-4 are membrane-associated proteins that localize at the inner nuclear membrane and
92 provide anchoring points for heterochromatin (*13, 28*). In contrast, PRR14 is a nuclear lamina-
93 associated protein that is found primarily at the nuclear lamina with a much smaller fraction observed
94 in the nucleoplasm. The observation that PRR14 localization is not strictly restricted to the nuclear
95 periphery (*18, 29*) indicates that PRR14 association with the nuclear lamina is dynamic, and that the
96 mechanism of chromatin tethering to the nuclear lamina via PRR14 could be different from that of
97 LBR and CEC-4.

98 PRR14 was originally identified as an epigenetic repressor of gene expression (*30*). Further studies
99 demonstrated that PRR14 localizes at the nuclear lamina, specifically in association with Lamin A/C
100 (*18*). PRR14 has a 120-residue lamina-binding domain (LBD) that includes two independent lamina-
101 binding motifs, both of which have been reported to be phosphoregulated (*29*). PRR14 also contains
102 an HP1-binding motif in the N-terminal portion of the protein, and the PRR14-HP1 interaction has
103 been shown to be required for PRR14 to bind chromatin (*31*). The C-terminus of the protein has a
104 proposed regulatory function and includes a Tantalus domain with a Protein Phosphatase 2 Subunit
105 Alpha (PP2A) binding motif. Interaction with PP2A is understood to regulate phosphorylation of the
106 LBD and thus association of the protein with the nuclear lamina. While the domain structure of PRR14
107 has been described and several interacting proteins identified, the spatial dynamics of PRR14 in the
108 nucleus and its ability to organize heterochromatin at the nuclear periphery has yet to be investigated.

109 Here we demonstrate that PRR14 organizes, specifically, H3K9me3-modified heterochromatin at the
110 nuclear lamina, but not H3K9me2. Our experimental results show that PRR14 is dynamically
111 associated with the nuclear lamina and heterochromatin, and is capable of reorganizing H3K9me3-
112 modified heterochromatin in interphase, independent of mitosis. We have identified a second HP1-
113 binding motif in the N-terminus of the protein and show that it stabilizes PRR14 association with
114 heterochromatin. Interrogation of the ability of PRR14 to bind the individual isoforms of
115 heterochromatin protein 1 (HP1) revealed an *in vivo* preference for HP1α and HP1β. Fluorescent
116 recovery after photobleaching (FRAP) experiments demonstrated that PRR14 interactions with the
117 nuclear lamina are relatively stable as compared with the more dynamic interactions of PRR14 with
118 heterochromatin via HP1. Finally, our super-resolution imaging of PRR14 localization in the nucleus
119 indicate that PRR14 is predominantly located at the nuclear lamina where, we predict, it provides an
120 anchoring surface for HP1-associated, H3K9me3-modified chromatin. Combined, our results
121 demonstrate the molecular mechanism of heterochromatin organization by PRR14 and suggest a
122 dynamic model of heterochromatin tethering to the nuclear periphery.

123 **RESULTS**

124 **PRR14 specifically tethers H3K9me3-modified heterochromatin to the nuclear lamina**

125 *PRR14* encodes a protein with modular domains that bind to heterochromatin, via HP1, or to the
126 nuclear lamina (Fig. 1A). Given this domain structure, it has been postulated that PRR14 functions to
127 tether heterochromatin to the nuclear lamina (Fig. 1B) and this model is supported by loss-of-function
128 experiments (*18*). It has not yet been established whether PRR14 shows specificity for
129 heterochromatin with particular histone modifications to be bound and positioned at the nuclear
130 lamina. We tested the ability of PRR14 to tether H3K9me2- and H3K9me3-modified heterochromatin
131 to the nuclear lamina in light of recent reports showing separate functions for H3K9me2 and H3K9me3
132 chromatin modifications (*12, 32, 33*).

133 Expression of exogenous GFP-tagged PRR14 in two different cell types, murine NIH/3T3 and human
134 IMR-90, resulted in a significant increase of H3K9me3-modified heterochromatin found at the nuclear
135 lamina (Fig. 1C-D). This repositioning of H3K9me3-modified heterochromatin to the nuclear lamina
136 was observed to be greater in NIH/3T3 cells, probably due to the lower baseline amount of H3K9me3
137 at the nuclear periphery prior to overexpression of PRR14. Unlike H3K9me3-modified
138 heterochromatin, H3K9me2-marked heterochromatin did not show a statistically significant change in
139 the fraction at the nuclear lamina (Fig. S1).

140 To determine if the relocalization of H3K9me3-modified heterochromatin depends on PRR14's HP1-
141 binding domain-mediated heterochromatin interaction, we used the previously described mutant of
142 HP1-binding motif (LAVVL) with residues V54 and V55 substituted to glutamic acid (54-55EE).
143 Unlike exogenous expression of wild-type PRR14, expression of the mutant PRR14 54-55EE
144 construct did not alter the localization of H3K9me3- or H3K9me2-marked heterochromatin; rather
145 cells expressing PRR14 54-55EE were similar to mock-transfected cells (Fig. 1C-D, Fig. S1).
146 Combined, these results demonstrate that PRR14 specifically tethers H3K9me3-modified
147 heterochromatin to the nuclear lamina.

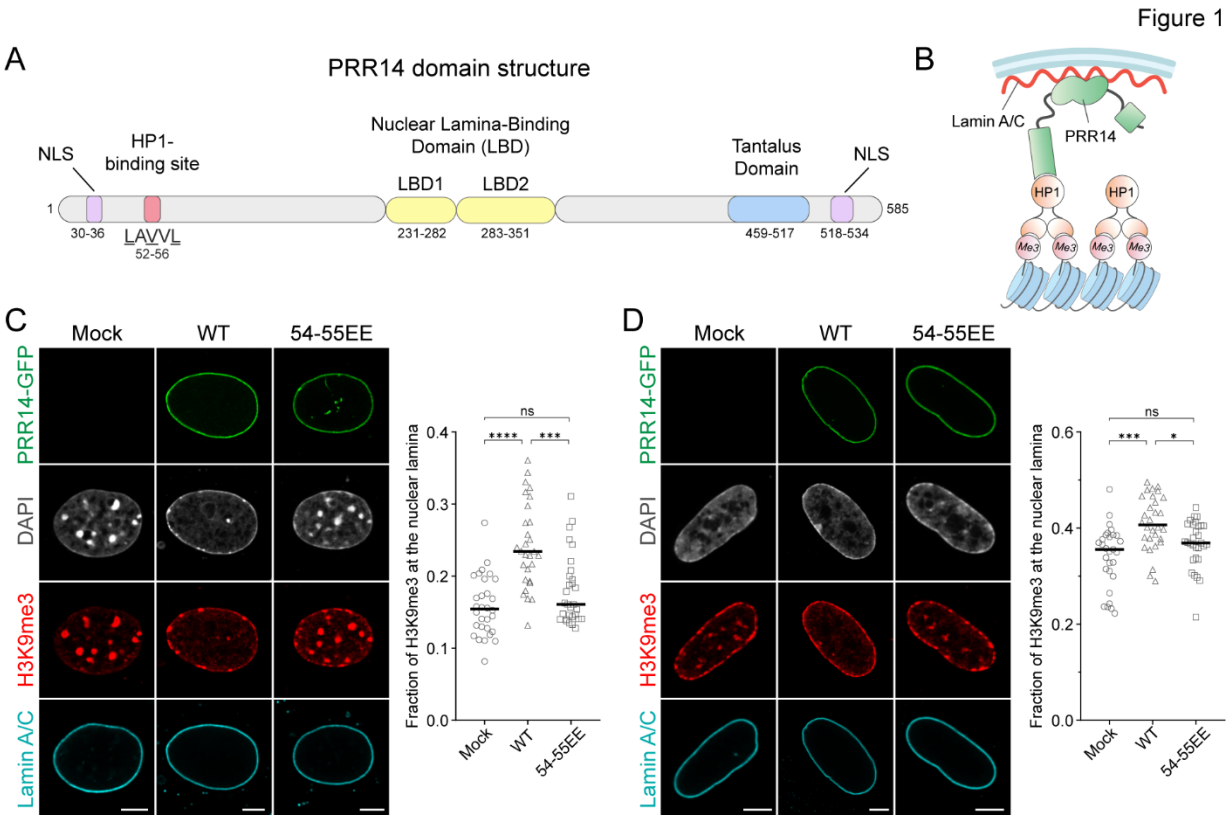

148

149 **Figure 1. PRR14 specifically tethers H3K9me3-modified heterochromatin to the nuclear lamina.** Schematic
150 illustrations of **(A)** PRR14 domain organization, functional motifs and **(B)** mechanism of heterochromatin tethering to the
151 nuclear lamina. Amino acid residues in (A) refer to human protein coordinates. NLS, nuclear localization signal. **(C-D)**
152 Representative confocal images of (C) murine NIH/3T3 and (D) human IMR-90 cells expressing GFP-tagged PRR14
153 constructs (green): wildtype (WT) or mutant V54E, V55E (54-55EE) and stained for H3K9me3 (red) and Lamin A/C (cyan).
154 DAPI counterstain shown in gray. Dot plots show the fraction of H3K9me3 signal at the nuclear lamina. n ≥ 30 cells per
155 condition. Lines on dot plot show median values. Statistical analysis was performed using ANOVA Kruskal-Wallis test with
156 Dunn's multiple comparisons; ****p < 0.0001, ***p < 0.001, *p < 0.05, ns: not significant. Scale bars 5μm.
157

158 **PRR14 organizes heterochromatin at the nuclear lamina in interphase nuclei independent of**
159 **mitosis**

160 PRR14 was previously reported to bind chromatin at early anaphase onset prior to nuclear lamina
161 formation (*18*). Later in telophase, chromatin bound by PRR14 was observed to associate with newly
162 formed nuclear lamina, and it was therefore proposed that PRR14 might play a role in re-establishing
163 peripheral heterochromatin at mitotic exit (*31*). We sought to test whether mitosis is required for
164 PRR14 to reorganize H3K9me3-modified heterochromatin in the nucleus.

165 NIH/3T3 cells expressing PRR14-GFP were assayed for changes in H3K9me3-modified
166 heterochromatin localization following a double thymidine block to arrest the cell cycle and prevent
167 mitosis (Fig. S2, see Methods). PRR14 overexpression in both cycling and arrested cells resulted in a
168 significant increase in the fraction of H3K9me3-modified heterochromatin at the nuclear lamina with
169 no significant difference between untreated and thymidine-treated cells (Fig. 2). Similar levels of

170 H3K9me3 at the nuclear periphery of arrested and cycling cells with PRR14 overexpression suggests
171 that PRR14 can tether heterochromatin in interphase nuclei and organize heterochromatin at the
172 nuclear lamina independent of mitosis.

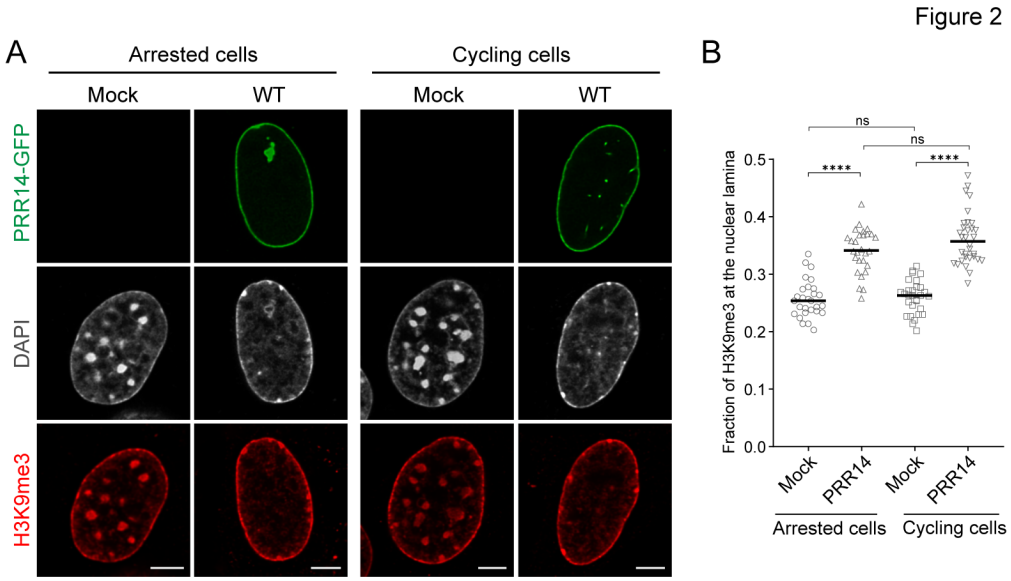

173

174 **Figure 2. PRR14 organizes H3K9me3-modified heterochromatin at the nuclear lamina in interphase nuclei**
175 **independent of mitosis.** (A) Representative confocal images of cell cycle-arrested and cycling murine NIH/3T3 cells
176 expressing WT GFP-tagged PRR14 constructs (green), stained for H3K9me3 (red). DAPI counterstain shown in gray. (B)
177 Dot plot shows the fraction of H3K9me3 signal at the nuclear lamina. Lines on dot plot show median values. n ≥ 30 cells
178 per condition. Statistical analysis was performed using ANOVA Kruskal-Wallis test with Dunn's multiple comparisons; ****p
179 < 0.0001, ns: not significant. Scale bars 5μm.
180

181 **PRR14 has a second HP1-binding site which stabilizes PRR14-heterochromatin interactions**

182 The LAVVL motif at the N-terminus of PRR14 (aa 52-56) is a variation of HP1-binding motif LxVxL.
183 Substitution of key residues within this motif – V54E, V55E (LAEEL), results in a dramatic decrease
184 of PRR14 association with chromatin (Fig. 1) (*18*). Through motif scanning of the remainder of the
185 protein, a second evolutionary conserved LxVxL sequence was identified within PRR14: LVVML, at
186 amino acids 153-157 (Fig. 3A), just beyond the region that was originally implicated as the chromatin-
187 binding domain (aa 1-135, (*18*)). We sought to determine if this site could also contribute to
188 heterochromatin binding.

189 To compare the functions of the first and putative second HP1-binding motifs of PRR14, we made
190 GFP-tagged PRR14 constructs encoding only the N-terminal 212 amino acids of the protein that
191 terminate before the lamina-binding domain (LBD) (Fig. 3B). In addition to a wild-type version, we
192 made GFP-tagged PRR14 1-212 constructs with amino acid substitutions that mutate the first (V54E,
193 V55E), the second (V154E, V155E) or both HP1-binding motifs (V54E, V55E, V154E, V155E),
194 denoted 54-55EE, 154-155EE and double mutant (DM), respectively (Fig. 3B).

We introduced the wild-type and mutant 1-212 fragments of PRR14 into NIH/3T3 cells, and as expected, the wild-type fragment showed consistent colocalization with chromocenters and heterochromatic regions in the nucleus that are known to be marked with the H3K9me3 histone modification (*34*) (Fig. 3C). The PRR14 1-212 fragment, which lacks the Lamina-Binding Domain (LBD), was not observed at the nuclear periphery (Fig. 3C).

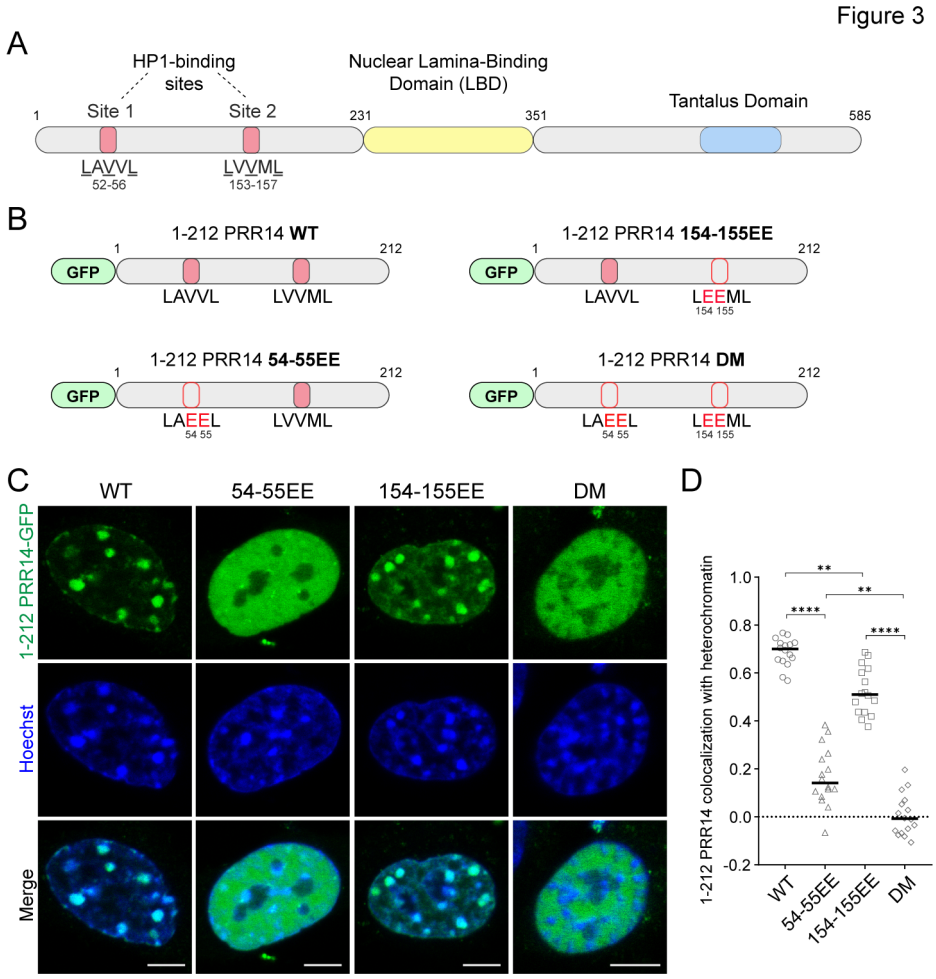

Figure 3. PRR14 HP1-binding site 1 shows strong heterochromatin binding and is essential for PRR14-heterochromatin association, while HP1-binding site 2 has much weaker heterochromatin binding. (A) Schematic illustrations of PRR14 domain organization and HP1-binding site motifs: LAVVL (aa 52-56) and LVVML (aa 153-157). **(B)** Schematic representation of GFP-tagged PRR14(1-212) fragments including the heterochromatin-binding domain of PRR14 with indicated amino acid substitutions in key residues of HP1-binding motifs. DM, double mutant. **(C)** Representative confocal images of murine NIH/3T3 cells expressing indicated WT or mutant GFP-tagged PRR14(1-212) constructs (green), counterstained with Hoechst (blue). **(D)** Dot plot shows the Pearson's correlation of Hoechst staining and GFP-PRR14 signal for each PRR14(1-212) construct indicating degree of colocalization of PRR14 with heterochromatin regions. n ≥ 16 cells per condition. Lines on the dot plot show median values. Statistical analysis was performed using ANOVA Brown-Forsythe and Welch test with Dunnett's multiple comparisons; ****$p < 0.0001$, **$p < 0.01$. Scale bars 5μm.

Substitution of amino acids in HP1-binding site 1 of PRR14 1-212 resulted in a dramatic decrease of PRR14 co-localization with heterochromatin as visualized by Hoechst staining. Expression of the 54-55EE mutant resulted in a diffused localization in the nucleus and minimal colocalization with

heterochromatin (Fig. 3C-D). In contrast, the 154-155EE mutant of HP-binding site 2 retained significant association with heterochromatin (Fig. 3C-D). Notably, co-localization of the PRR14 154-155EE mutant with heterochromatin was not as strong as that of the WT fragment and a measurable level of signal was observed in the nucleoplasm of cells expressing 154-155EE that was barely detectable in WT-expressing cells (Fig. 3C-D). Mutation of both HP1 binding sites (DM) shows complete absence of colocalization with heterochromatin (Fig. 3C-D). Taken together, these results demonstrate that HP1-binding site 1 plays the major role in heterochromatin binding, while HP1-binding site 2 contributes to a lesser degree to PRR14 interactions with heterochromatin. This is consistent with the observations that both PRR14 54-55EE and PRR14 DM lack the ability to efficiently tether heterochromatin to the nuclear lamina (Fig. 1C-D, Fig. S3). Overall, our data suggest that the second HP1-binding site, alone, is not sufficient for robust PRR14-heterochromatin binding in our assays, but may play a contributing role to the overall association of PRR14 with chromatin.

To further test if the second HP1-binding site affects heterochromatin binding, we performed fluorescent recovery after photobleaching (FRAP) experiments. We probed the association of the PRR14 1-212 fragment with large heterochromatin regions represented by chromocenters which, in murine cells, are known to be highly enriched for the H3K9me3 histone modification (*34*). There was a rapid recovery of the GFP-PRR14 signal following photobleaching of a single chromocenter in cells expressing the wild-type PRR14 1-212 fragment (Fig. 4A, Fig. S4). Normalized fluorescent recovery at photobleached regions was very high, with about 15% average immobile fraction of WT PRR14 1-212 fragment on heterochromatin (Fig. 4B-D). The average recovery half-time for WT PRR14 1-212 fragment was 4.5 seconds (Fig. 4C). This suggests a very rapid exchange and dynamic association of PRR14 with heterochromatin.

The 1-212 PRR14 154-155EE construct demonstrated similar dynamics of heterochromatin association but with a significantly lower average recovery half-time of 2.5 seconds (Fig. 4, Fig. S4). Thus, the interaction of PRR14 154-155EE is even more dynamic than that of WT PRR14, consistent with a role for the second HP1-binding site in stabilizing the overall association of PRR14 with chromatin.

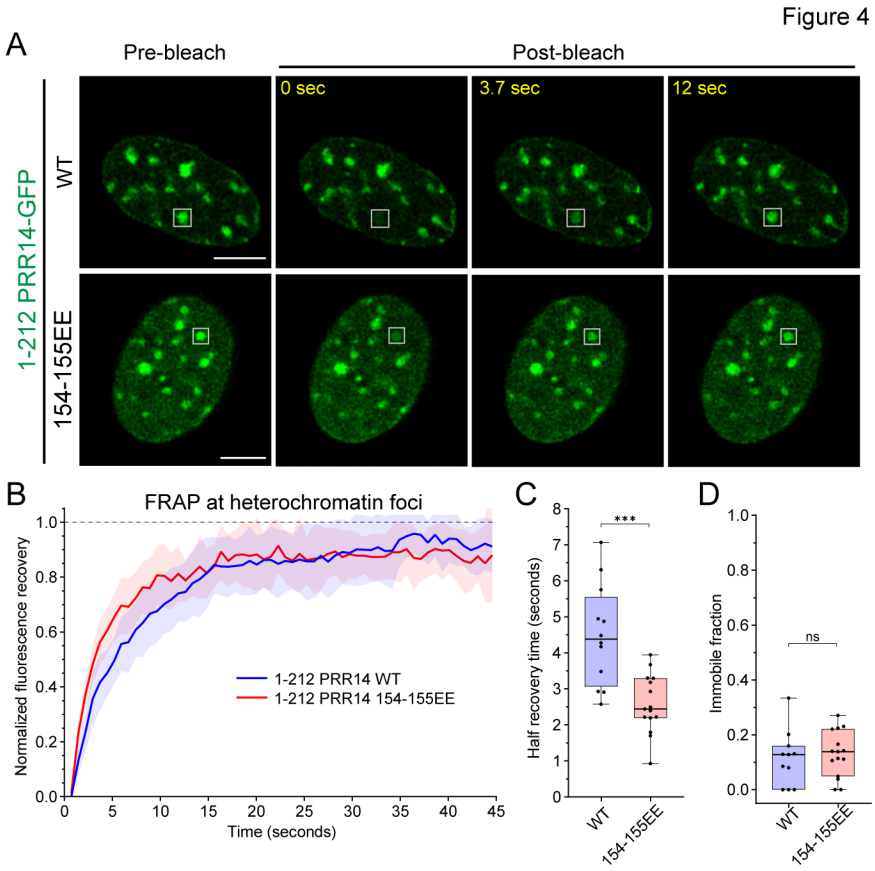

Figure 4. PRR14 HP1-binding site 2 stabilizes PRR14-heterochromatin interactions. (A) Representative confocal images of fluorescent recovery after photobleaching (FRAP) assay for PRR14(1-212) WT and 154-155EE mutant constructs. White boxes indicate the bleached area. **(B)** Line graph shows normalized fluorescent recovery over time after photobleaching in the areas indicated in (A) in cells expressing PRR14(1-212) WT (blue) or 154-155EE mutant (red). Line graph shows mean values with standard deviations displayed as shading. **(C)** Box plots show distributions of recovery half-times for indicated PRR14 (1-212) constructs. **(D)** Box plots show distributions of immobile fractions for indicated constructs. n ≥ 12 cells per condition. Box plots show median, 25th and 75th percentiles. Whiskers show minimum to maximum range. Statistical analysis was performed using Mann-Whitney test. ***$p < 0.001$, ns: not significant. Scale bars 5μm.

PRR14 binding preference for HP1 isoforms

PRR14 specificity for chromatin binding is mediated by its interactions with HP1 proteins. We sought to identify whether there is specificity with regard to which HP1 isoforms are bound by PRR14. Given the low solubility of full-length PRR14, we used PRR14 1-212 fragments in immunoprecipitation assays to assess the specificity of PRR14-HP1 interaction. Using anti-GFP antibodies GFP-PRR14 was immunoprecipitated from cells expressing WT GFP-PRR14 1-212 and the co-immunoprecipitated proteins were subjected to Western blot analysis for HP1 isoforms. All three HP1 isoforms were immunoprecipitated, suggesting that each can interact with PRR14 (Fig. 5A, Fig. S5).

We next sought to determine the specificity for each HP1-binding site of PRR14 by comparing the co-precipitating proteins of WT, 54-55EE, 154-155EE and DM PRR14 1-212 fragments (see Figure 3B). The interactions between PRR14 and all 3 HP1 isoforms was markedly reduced in cells expressing

263 PRR14 HP1-binding site 1 mutant (54-55EE), although a small amount of residual binding to HP1γ
264 was retained (Fig. 5A-B). Substitutions in HP1-binding site 2 (154-155EE) did not reduce the ability
265 of PRR14 to interact with any of the HP1 isoforms (Fig. 5A-B). Analysis of the double mutant (DM)
266 showed complete lack of HP1-PRR14 interaction (Fig. 5A-B). These results are consistent with a
267 dominant role for HP1 binding site 1 as a mediator of PRR14 interaction with all 3 HP1 isoforms, and
268 an apparently small contribution of HP1 binding site 2 to the interaction of PRR14 with HP1γ.

269 Since the exogenous expression of full-length PRR14 resulted in relocalization of H3K9me3-modified
270 heterochromatin to the nuclear lamina, we next asked whether overexpression of full-length PRR14
271 led to an increase in the amount of any of the HP1 isoforms at the nuclear periphery. In murine
272 NIH/3T3 cells transfected with full-length PRR14, we examined the localization of each of the HP1
273 isoforms. HP1α and HP1β are associated with heterochromatin in untransfected cells, and there was
274 a significant increase of both of these HP1 isoforms at the nuclear lamina in PRR14-overexpressing
275 cells (Fig. 5C, D, Fig. S6). HP1γ, less tightly associated with heterochromatin and known to organize
276 euchromatin (*24, 25*), appears more diffuse in the nucleoplasm of untransfected cells than the other
277 isoforms (Fig 5C). Overexpression of PRR14 resulted in little change in HP1γ localization (Fig. 5C,
278 D). Consistent with its reduced interaction with H3K9me3-modified heterochromatin, PRR14 54-
279 55EE overexpression did not reposition HP1α or HP1β and had a small but significant effect on HP1γ
280 (Fig. 5C-D). No relocalization of HP1γ was seen upon overexpression of the DM construct (Fig. 5C-
281 D). Given the minor effect of PRR14 overexpression on HP1γ, we tested if HP1γ participate in PRR14-
282 chromatin interaction. Knockdown of HP1γ resulted in decrease of PRR14 association with chromatin
283 (Fig. S7). This result in consistent with a role for the HP1-binding site 2 (Fig. 3) that preferably binds
284 HP1γ.

285 Overall, our data demonstrate that PRR14 HP1-binding site 1 (LAVVL, aa 52-56) binds all 3 HP1
286 isoforms and is essential for heterochromatin tethering to the nuclear lamina (Figs. 1 and 5). PRR14
287 HP1-binding site 2 (LVVML, aa 153-157) exhibits preferential binding for HP1γ (Fig. 5) and may
288 function to augment overall PRR14 association with chromatin (Fig. 4).

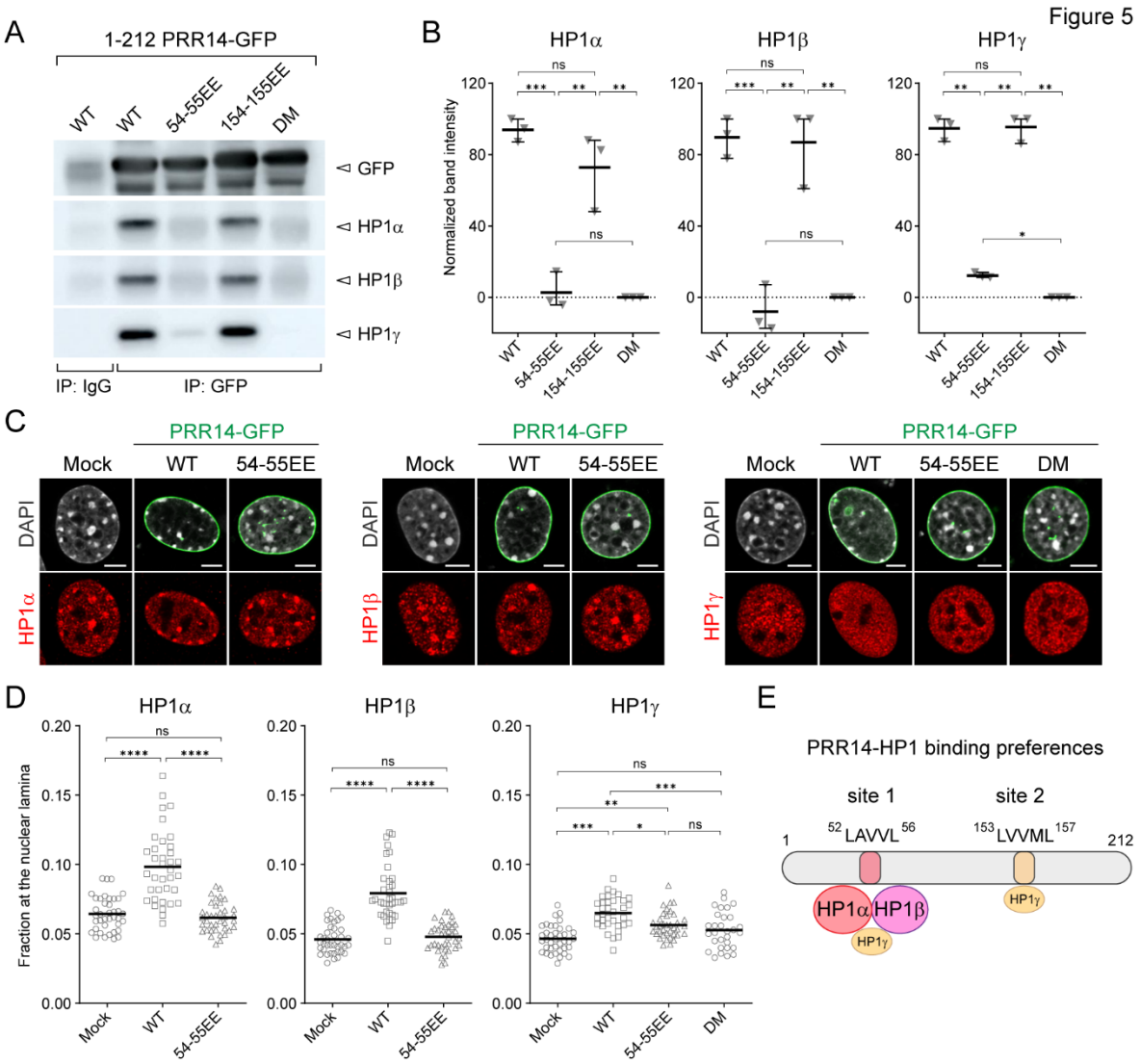

Figure 5. PRR14 binds all three HP1 isoforms *in vitro*, but *in vivo* shows more specific nuclear lamina tethering of chromatin marked with HP1α and HP1β. (A) Lysates of 293T cells expressing indicated GFP-PRR14 (1-212) constructs were immunoprecipitated (IP) with anti-GFP antibody and analyzed by Western blotting using antibodies against the indicated HP1 isoform. IgG serves as an isotype control for non-specific antibody interactions. **(B)** Dot plots show normalized intensities of indicated HP1 signal after immunoprecipitation with anti-GFP antibodies. n = 3 independent immunoprecipitations. Lines on dot plots show average values. Whiskers show range. **(C)** Representative confocal images of murine NIH/3T3 cells mock transformed or expressing GFP-PRR14 WT or mutant constructs (green) and stained for HP1 isoforms (red) as indicated. DAPI counterstain shown in gray. **(D)** Dot plots show ratio of indicated HP1 protein signal at the nuclear lamina for murine NIH/3T3 cells expressing GFP-PRR14 WT or mutant constructs as indicated. Lines on dot plots show average values. n ≥ 30 cells per condition. **(E)** Schematic illustration of PRR14-HP1 binding site 1 and site 2 preferences for HP1 isoforms. Statistical analysis was performed using paired ANOVA test with Geisser-Greenhouse correction for panel B and ANOVA Kruskal-Wallis test with Dunn's multiple comparisons for panel D; ****p < 0.0001, ***p < 0.001, **p < 0.01, *p < 0.05, ns: not significant. Scale bars 5μm.

PRR14 association with the nuclear lamina is independent of heterochromatin binding

PRR14 association with HP1/heterochromatin is highly dynamic, as described above (Fig. 4). Next, we sought to characterize PRR14 interactions with the nuclear lamina, which have been shown to occur between the PRR14 lamina-binding domain (LBD) and Lamin A/C (*18*). The relative

308 contributions of PRR14-nuclear lamina and PRR14-heterochromatin binding for nuclear lamina
309 localization were investigated using FRAP. We assayed the dynamics of PRR14 at the nuclear lamina
310 for both the full-length protein and the isolated PRR14 LBD (residues 231-351) (Fig. 6A). WT PRR14
311 protein exhibited a high level of immobile fraction at the nuclear lamina, with an average of 55%, and
312 the recovery half-time of PRR14 at the nuclear lamina averaged 25 seconds (Fig. 6B-C). By way of
313 comparison, the half-recovery time for Lamin A/C at the lamina has been reported to be from 10 to 60
314 minutes (*35*), suggesting that PRR14 interactions with the lamina are relatively dynamic.

315 In contrast to full-length PRR14, the LBD fragment demonstrated very different dynamics with only
316 a small immobile fraction (<15%) and an average half-recovery time of 15 seconds (Fig. 6A-C). The
317 LBD fragment lacks both the N-terminal chromatin-binding region and the C-terminal regulatory
318 region. This suggests that the full-length protein is stabilized at the nuclear lamina through additional
319 interactions that result in a significant immobile fraction.

320 We tested if interaction with HP1 proteins and/or chromatin contribute to PRR14 retention at the
321 nuclear periphery by assaying the dynamics at the nuclear lamina of full-length PRR14 constructs with
322 HP1-binding site mutants (54-55EE and DM), We found no significant differences between these
323 mutant forms and WT PRR14 in terms of half-recovery time or amount of immobile fraction (Fig. 6D-
324 E, Fig. S8). This suggests that PRR14 dynamics at the nuclear periphery are independent of PRR14-
325 HP1/heterochromatin binding.

326 Direct comparisons of PRR14 association with heterochromatin (Fig. 4) and with the nuclear lamina
327 (Fig. 6) indicate that PRR14 association with the nuclear periphery is less dynamic than the association
328 of PRR14 with heterochromatin (Fig. S9). Thus, our results support a model in which PRR14 primarily
329 occupies the nuclear lamina where it performs transient attachment to HP1-associated
330 heterochromatin.

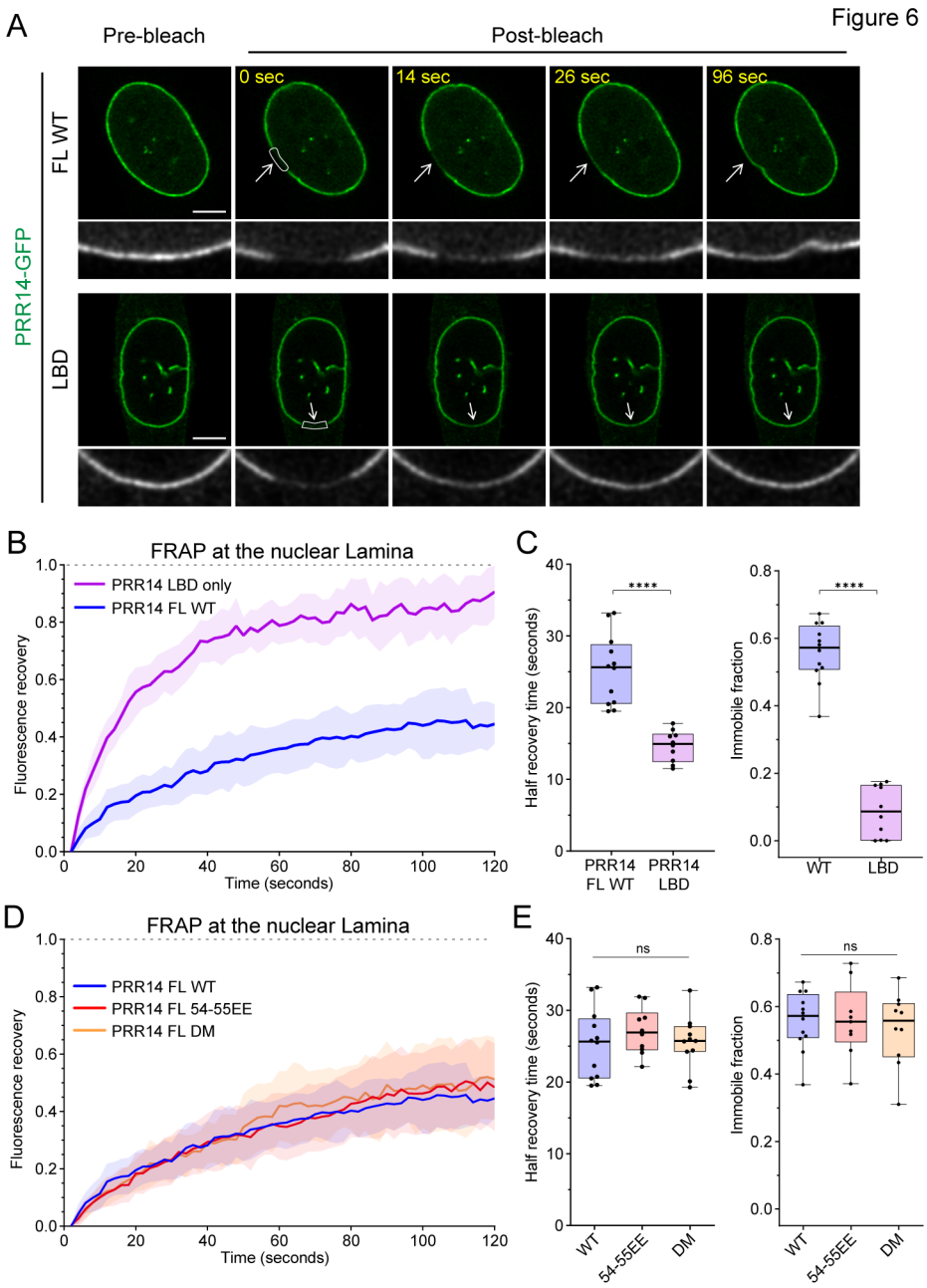

Figure 6. PRR14 association with the nuclear lamina is dynamic and independent of PRR14-heterochromatin binding. (A) Representative confocal images of fluorescence recovery after photobleaching (FRAP) assay of WT GFP-PRR14 full-length (PRR14 FL) and lamina-binding domain (LBD) constructs. White boxes indicate bleached area. **(B)** Line graph shows normalized FRAP signal in the areas indicated with boxes in (A) for PRR14 full-length (blue) and PRR14 LBD-only fragment (purple). **(C)** Box plots show distributions of recovery half-time (left) and immobile fraction (right) for indicated constructs. **(D)** Line graph shows normalized FRAP signal in the areas indicated with boxes (Fig. S6) for PRR14 FL WT (blue) and mutant full-length constructs 54-55EE (red), or double mutant (DM; yellow). **(E)** Box plots show distributions of recovery half-time (left) and immobile fraction (right) for indicated constructs. n ≥ 12 cells per condition. Line graphs show mean values with standard deviations displayed as shading. Box plots show median, 25th and 75th percentiles; whiskers show minimum to maximum range. Statistical analysis was performed using Mann-Whitney test and analysis of variance (ANOVA) Kruskal-Wallis test with Dunn's multiple comparisons. ****$p < 0.0001$, ns: not significant. Scale bars 5μm.

344 **PRR14 at the nuclear lamina creates a surface for heterochromatin anchoring**

345 We used super-resolution microscopy to visualize the location of PRR14 in the nucleus, examining
346 both the nuclear lamina and the nucleoplasm. Localization of PRR14, Lamin A/C and H3K9me3 were
347 subjected to Stochastic Optical Reconstruction Microscopy (STORM) and Figure 7 shows
348 representative images of a middle plane (Fig. 7A) and a bottom plane at the periphery (Fig. 7B) of the
349 nucleus. PRR14 is observed predominantly at the inner nuclear membrane (INM) forming a similar
350 meshwork as Lamin A/C on the INM surface (Fig. 7B), consistent with analyses of our confocal
351 images. A much smaller fraction of PRR14 was observed in the nucleoplasm (Fig. 7A). Nucleoplasmic
352 PRR14 is almost uniformly distributed and lacks noticeable clusters specific for H3K9me3-modified
353 heterochromatin (Fig. 7A, B). In comparison, H3K9me3 is apparent as clusters of heterochromatin
354 both at the nuclear lamina and in the nucleoplasm (Fig. 7A, B). No such clustering was observed for
355 PRR14, suggesting that the nucleoplasmic fraction of PRR14 does not strongly associate with
356 heterochromatin away from the nuclear lamina surface. Such localization of PRR14 at the nuclear
357 periphery creates a layer of molecules that are capable of binding H3K9me3-modified
358 heterochromatin associated with HP1 as it comes into contact with the nuclear periphery.

359 The results presented here suggest a model in which PRR14 creates a meshwork at the nuclear lamina
360 that organizes H3K9me3-modified heterochromatin at the nuclear periphery through dynamic
361 association with HP1 (Fig. 7C). This PRR14 meshwork might be thought of as a “sticky” surface, or
362 “Velcro”, that allows H3K9me3-modified heterochromatin bound by HP1 to become transiently
363 attached to the nuclear lamina.

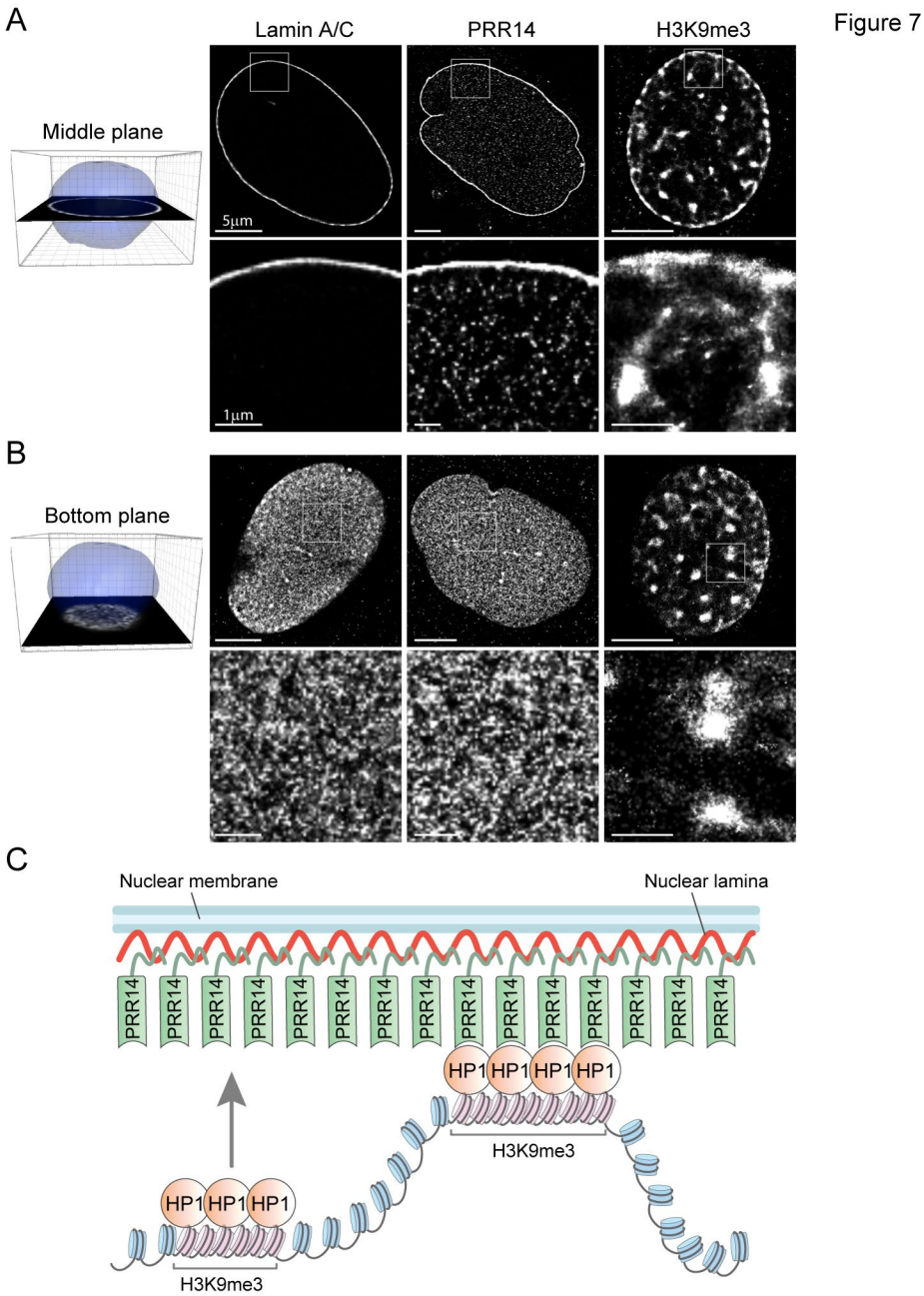

364

365 **Figure 7. PRR14 is predominantly localized at the nuclear lamina where it creates a surface for anchoring**
366 **HP1/H3K9me3-modified heterochromatin. (A)** Representative super-resolution stochastic optical reconstruction
367 microscopy (STORM) images showing localization of Lamin A/C, PRR14 and H3K9me3 in the middle plane of nuclei of
368 NIH/3T3 cells. White boxes (top panels) show zoomed areas (bottom panels). **(B)** Representative STORM images showing
369 localization of Lamin A/C, PRR14 and H3K9me3 at the bottom plane of nuclei of NIH/3T3 cells. **(C)** A model illustrating the
370 mechanism for PRR14 tethering H3K9me3-modified chromatin to the nuclear lamina through interaction with HP1. Scale
371 bars: 5μm (top panels) and 1μm (bottom panels).
372

373 **DISCUSSION**

374 In this study, we have demonstrated that PRR14 functions at the nuclear lamina to specifically organize
375 H3K9me3-modified heterochromatin. We observed no evidence of interaction between PRR14 and
376 H3K9me2, an established a mark of peripheral heterochromatin (*12*). We showed that PRR14 is
377 associated with the nuclear lamina and heterochromatin in interphase, and is able to reorganize
378 H3K9me3-modified heterochromatin independent of mitosis. Further, we showed that PRR14 tethers
379 chromatin to the nuclear lamina via heterochromatin protein 1 (HP1), primarily isoforms HP1α and
380 HP1β, although our experiments indicate that PPR14 can bind the HP1γ isoform as well. We have also
381 mapped a second HP1-binding motif at the N-terminal end of the protein. This site is not sufficient for
382 independent HP1 binding, but may function to strengthen PRR14 association with chromatin. Analysis
383 of PRR14 association dynamics with the nuclear lamina and chromatin, in addition to super-resolution
384 imaging of PRR14 localization in the nucleus, have led us to propose a refined model of
385 heterochromatin tethering to the nuclear periphery. Taken together, our results suggest a mechanism
386 through which PRR14 organizes heterochromatin at the nuclear lamina and provide new insights into
387 the organization of peripheral chromatin.

388 Only a few chromatin tethers have been described to date (reviewed in (*15*)). The list of widely
389 expressed tethers is limited to LBR and PRR14 in mammals (*16, 18*) and CEC-4 in *C. elegans* (*13*).
390 These tethers are expressed in most cell types and have a similar mechanism of action: all of them
391 specifically interact with chromatin bearing H3K9 methyl-modified histones. PRR14 stands out
392 among known tethers as LBR and CEC-4 are integrated nuclear envelope proteins with restricted
393 localization in the nuclear membrane, while PRR14 is a nuclear lamina-associated protein that has
394 dynamic localization at the nuclear periphery.

395 A notable feature of PRR14 is the duplication of key functional elements. The protein has two NLS
396 signals, two lamina-association motifs, and two HP1-binding sites (*18, 29*). As is frequently seen in
397 evolution, these duplicated regions are not identical. We have yet to determine whether each of these
398 regions provides functional redundancy, modified function, or has already lost their original function
399 through mutational drift. Such protein redundancy might ensure protein function in multiple cell types
400 as well as additional levels of regulation of protein function(s). Our earliest PRR14 study demonstrated
401 that each NLS is independently sufficient to transport PRR14 into the nucleus, but with lesser
402 efficiency singly than when combined (*18*). Therefore, two NLS sequences might serve to efficiently
403 deliver PRR14 in the nucleus. Similar function is observed for the LBD where each lamina-associated
404 domain is able to position the protein to the nuclear lamina independently, but much less efficiently

405 than that observed when both are intact (*29*). Furthermore, LBD-1 region has been shown to be
406 regulated via phosphorylation whereas this has not been demonstrated for LBD-2 (*29*). Such complex
407 organization of the lamina-binding domain allows for regulation of PRR14 association with the
408 nuclear lamina, thus regulating heterochromatin tethering capabilities of PRR14. In this study, we
409 identified a second HP1-binding motif (LVVML, aa 153-157), located near the first HP1-binding site
410 (LAVVL, aa 52-56) in the N-terminus of the protein. Both motifs are a variation of LxVxL sequence
411 which binds the chromo-shadow domain (CSD-CSD) pocket of HP1 (*36*) and are not identical (Fig.
412 3A). The first HP1-binding motif (LAVVL) of PRR14 was described previously and experiments with
413 substitution of the key amino acids residues in this motif showed a dramatic reduction of PRR14-
414 chromatin association (*18*). Here, we confirmed that LAVVL motif of binding site 1 plays a major
415 function in chromatin binding and tethering (Figs. 1,3, and 5), while the second LVVML motif of
416 binding site 2 has a supportive function in PRR14 association with heterochromatin (Figs. 3-4). We
417 speculate that a variation in sequences of these two motifs accounts for a preference for specific HP1
418 isoforms as well as the strength of the association with HP1.

419 As was recently demonstrated by Machida et al, HP1 dimers can bind H3K9me3 histone modifications
420 at two distinct nucleosomes, and thus function to compact heterochromatin by bringing nucleosomes
421 together (*37*). We speculate that an ability of PRR14 to bind two HP1 dimers could also result in
422 chromatin compaction. If this hypothesis is correct, HP1-bound heterochromatin would undergo
423 further compaction when it interacts with PRR14 at the nuclear periphery. We further speculate that
424 two HP1-binding sites of PRR14 might have an HP1-locking function, similar to that previously
425 described for SENP7 by Romeo et al (*38*), in which two HP1 interaction motifs restrict HP1 mobility
426 at heterochromatin, thereby locking HP1 molecules docked on H3K9me3-modified nucleosomes to
427 promote stable HP1 accumulation. Further studies are needed to elucidate the role of HP1 in specifying
428 chromatin regions for localization at the nuclear periphery.

429 Previously, PRR14 was reported to bind HP1α (*18, 39*). Here we demonstrate that PRR14 can bind
430 all HP1 isoforms, although tethering to the nuclear periphery in the context of PRR14 overexpression
431 was observed largely for HP1α and HP1β isoforms (Fig. 5B). This agrees with the accepted function
432 for HP1α and HP1β in organizing heterochromatin, in contrast to the HP1γ isoform which has been
433 found in both heterochromatin and euchromatin regions (*24, 25*). Previous studies demonstrated that
434 HP1 isoforms can form heterodimers as well as homodimers (*25, 40, 41*). This feature of HP1 isoforms
435 makes it difficult to determine whether a homodimer of a single isoform or a heterodimer is bound by
436 PRR14. Specificity of PRR14 for chromatin binding via HP1 could be further complicated by various

437 HP1 dimers and post-translational modifications of HP1 (reviewed in (*22*)). Some HP1 interactions
438 with other binding partners utilize the same PxVxL-binding pocket or positions the HP1 dimer deep
439 inside the nucleosome, thus making HP1 unavailable for interaction with PRR14 (*22*). This agrees
440 with the relatively moderate effect of PRR14 overexpression on HP1 relocalization to the nuclear
441 lamina (Fig. 5). Our results provide evidence that PRR14 functions to organize H3K9me3-modified
442 heterochromatin decorated with HP1α/β at the nuclear lamina. Further studies are needed to identify
443 specific genomic regions that are organized at the nuclear periphery by PRR14. Such specificity could
444 be cell type-specific and dictated by a combination of multiple factors including relative levels of HP1
445 isoforms and PRR14.

446 PRR14 tethers heterochromatin regions enriched for the H3K9me3 histone modification, which is
447 known to mark silent genes and promoters, but is more abundant in repetitive heterochromatin regions
448 such as major and minor satellites, LINE elements etc. Localization of heterochromatin at the nuclear
449 periphery not only functions to efficiently repress expression of cellular genes and repetitive elements,
450 but has also been shown to have nongenetic functions to which PRR14 may contribute (*7*). PRR14
451 could organize repetitive heterochromatin marked with HP1/H3K9me3 at the nuclear periphery to
452 affect nuclear shape and stiffness. This putative PRR14 function is supported by our prior observations
453 that PRR14 knockdown results in nuclear shape defects (*18, 31*). However, we originally identified
454 PRR14 as an epigenetic repressor and demonstrated that PRR14 knockdown can activate
455 epigenetically silent genes (*30*). More recent studies aimed to address whether PRR14 is involved in
456 signaling pathways during tumorigenesis (*42*), but the mechanism by which PRR14 could perform
457 such functions is unclear. We speculate that PRR14 can serve as an epigenetic repressor by tethering
458 and thereby silencing genes at the nuclear lamina. A knockdown or mutation of PRR14, as well as
459 PRR14 phosphorylation (*29*), would result in release of genes from the nuclear periphery and
460 activation, similar to that previously described for genes released from lamina-associated domains
461 (LADs) (*5, 12, 14*).

462 Based on our data, we propose that the mechanism used by PRR14 to tether heterochromatin to the
463 nuclear lamina is regulated on multiple levels: 1) PRR14-chromatin binding is dictated by HP1 protein
464 isoforms; 2) PRR14-nuclear lamina association is regulated by phosphorylation of the lamina-binding
465 domain of PRR14; 3) spatial position of HP1/H3K9me3-modified heterochromatin is likely influenced
466 by PRR14 expression levels and the overall amount of PRR14 on the nuclear lamina surface.

467

468 The results presented here, in combination with our previous studies, suggest a dynamic model of
469 H3K9me3-modified heterochromatin organization at the nuclear periphery. In contrast to H3K9me2-
470 marked chromatin, which is nearly exclusively located at the nuclear lamina (Fig. S1) (*12, 43*),
471 H3K9me3-modified heterochromatin is observed at the perinucleolar heterochromatin and
472 chromocenters, in addition to the nuclear periphery (Figs. 1 and 7). Several studies have described the
473 dynamic behavior of heterochromatin, including that seen at the nuclear periphery, as it is exchanged
474 between the peripheral and perinucleolar compartments (*33*). This dynamic feature of H3K9me3-
475 modified chromatin is consistent with previous observations that peripheral heterochromatin could be
476 relocated to another heterochromatin compartment after mitosis (*44*). Based on our results, we propose
477 that PRR14 creates a surface at the nuclear lamina that is capable of anchoring heterochromatin with
478 which it comes into contact (Fig. 7C).

479

480 **MATERIALS AND METHODS**

481 **Cell lines**

482 Mouse NIH/3T3 (ATCC, cat# CRL-1658), human IMR-90 (ATCC, cat# CCL-186) and Lenti-X™
483 293T (Takara Bio, cat# 632180) cell lines were cultured in full-DMEM (Corning, cat# 10013CV)
484 supplemented with 10% FBS (Atlanta Biologicals, cat# S11150) and 1x Penicillin-Streptomycin
485 solution (ThermoFisher Scientific/Invitrogen, cat# 15140122). All cultured cell lines were routinely
486 tested for mycoplasma contamination every 3 months using a e-Myco VALID Mycoplasma PCR
487 Detection Kit (iNtRON Biotechnology, Inc., cat# 25239).

488 **Plasmids**

489 The human wild-type PRR14 expression construct pCMV6-AN-mGFP-PRR14 was previously
490 described (*18, 29*). pCMV6-AN-mGFP-PRR14 wild-type and HP1-binding domain mutants (site 1
491 mutant (54-55EE), site 2 mutant (154-155EE), and double mutant (54-55EE and 154-155EE)) were
492 made using site-directed mutagenesis. PRR14 1-212 aa fragments (wild-type and the HP1-binding
493 domain mutants, as described above) were amplified from the corresponding pCMV6-AN-mGFP-
494 PRR14 full-length vectors using Q5 Hot-start High-Fidelity Polymerase 2x Mix (New England
495 Biolabs, cat# M0494S) and the following primers containing HindIII and RsrII restriction sites
496 (Forward (HindIII): 5'- GCTTCTCAAGCTTGTACCATCCATGGACTTGCCCGG-3'; Reverse
497 (RsrII): 5' -TGCGATCGGTCCGCGCTTAGTCTGCAGGCAGAGC-3'). Then, PRR14 1-212 PCR
498 products were sub-cloned into the expression vector pCMV6-AN-mGFP using T7 ligase (New
499 England Biolabs, cat# M0318S) according to the manufacturer's instructions.

500 To make Doxycycline-inducible vectors, PRR14-GFP 1-212 wild-type and the HP1-binding domain
501 site 1 mutant (54-55EE) were amplified from the corresponding pCMV6-AN-mGFP-PRR14 full-
502 length vectors using Q5 Hot-start High-Fidelity Polymerase 2x Mix (New England Biolabs, cat#
503 M0494S) and the following primers containing EcoRI and AgeI restriction sites (Forward (EcoRI):
504 5'- ACTATAGGGCGGCCGGGAATTCGTCGACT -3'; Reverse (AgeI): 5' -
505 GATGTCGCGACCGGT TTAGTCTGCAGGCAGAGCAGA -3'). After that, PRR14-GFP 1-212
506 PCR products were sub-cloned into pLVX-TetOne-Puro (Takara Bio, cat# 631847) vector using T7
507 ligase (New England Biolabs, cat# M0318S) according to the manufacturer's protocol.

508 **Lentivirus production**

509 Lenti-X 293T cells were plated on a 6-well dish and grown to 80% confluent before transfection. To
510 make the lentiviruses containing Doxycycline-inducible PRR14 wt and 54-55EE mutant, 1.2 μg of
511 lentiviral vectors were premixed with 1.2 μg of packaging psPAX2 vector (Addgene, cat# 12260), and
512 0.75 μg of envelope pMD2.G vector (Addgene, cat# 12259) and transfected into Leni-X 293T cells

513 using Lipofectamine 3000 (ThermoFisher Scientific/Invitrogen, cat# L3000008) transfection reagent.
514 Supernatant containing lentiviruses was harvested 48- and 72-hours post-transfection, passed through
515 0.45 µm filter to eliminate contamination with Lenti-X 293T cells and cell debris, and pooled together.
516 The lentiviruses were used immediately to infect NIH/3T3 cells.

517 **Stable cell line production**

518 To generate a stable cell line expressing Doxycycline-inducible WT or 54-55EE mutant of 1-212
519 PRR14-GFP, NIH/3T3 cells were infected with the corresponding lentiviruses (1/5 – lentivirus/cell
520 culture medium) in the presence of 4 µg/mL polybrene (Sigma-Aldrich, cat# 107689). 4 days post-
521 infection, cells were split and selected for positive clones using 2 µg/mL puromycin for 5 days.

522 **Transient DNA and siRNA transfection**

523 Lipofectamine 3000 or FuGENE 6 transfection reagents (ThermoFisher Scientific/Invitrogen, cat#
524 L3000008; and Promega, cat# E2691) were used for transient delivery of PRR14 plasmids, in
525 accordance with the manufacturer's guidelines. For super-resolution and confocal imaging cells were
526 plated on 8-well ibidi µ-slides (ibidi, cat# 80826) or on 12x12 mm GOLD SEAL® glass coverslips
527 (Electron Microscopy Sciences, cat# 63786-01) correspondingly, then transfected at 50% confluency
528 and fixed 48 hours post-transfection (for STORM or IF) or imaged live (for FRAP or PRR14/DNA
529 co-localization analysis).
530 For siRNA transfection, Lipofectamine RNAiMAX transfection reagent (ThermoFisher
531 Scientific/Invitrogen, cat# 13778075) was used according to the manufacturer's protocol. siGENOME
532 pools of four siRNAs against Mouse Hp1γ or non-targeting siRNA control (Horizon
533 Discovery/Dharmacon, cat# M-044218-01-0005 and D-001206-13-05) at the final concentration of 50
534 nM were used. Doxycycline-inducible NIH/3T3 cells expressing WT of 54-55 EE mutant of 1-212
535 PRR14-GFP, described above, were plated on 8-well ibidi µ-slides. The next day, PRR14-GFP
536 expression was induced by adding 2 ug/mL Doxycycline (Sigma-Aldrich, cat# D9891-25g), and at the
537 same time, cells were transfected with the siRNAs. Live cell imaging was performed 72 hours post
538 siRNA transfection and the addition of Doxycycline. Right before the imaging, cells were
539 counterstained with 1 µg/mL of Hoechst 33342 (ThermoFisher Scientific/Invitrogen, cat# 62249) for
540 10 min. The imaging was performed using a 1x Live Cell Imaging Solution (ThermoFisher
541 Scientific/Invitrogen, cat# A14291DJ) and in a temperature and humidity-controlled microscope
542 chamber set at 37ºC.

543 **Cell cycle synchronization by a double thymidine block**

544 Cells were synchronized at the G1/S border using a double thymidine block as described previously
545 (*45*). In brief, NIH/3T3 cells were plated on 12x12 mm coverslips in 6-well plates (ThermoFisher

546 Scientific, cat# 140675). The next day cells were pre-treated with 2 mM Thymidine (Sigma-Aldrich,
547 cat# T9250-1G) and 5 hours later transfected with pCMV6-AN-mGFP-PRR14-WT or pCMV6-AN-
548 mGFP-PRR14-site 1 mutant (54-55EE) using FuGENE 6 transfection reagent in the presence of 2 mM
549 Thymidine in the culture medium to arrest cells in G1/S phase. Thirteen hours post-transfection,
550 Thymidine was removed from the medium and the cells were "released" for 9 hours by adding fresh
551 medium to initiate cell-cycle progression. To increase the percentage of G1/S arrested cells, a second
552 round of 2mM Thymidine treatment was performed for another 13 hours, and after that the cells were
553 either kept with Thymidine for additional 12 hours ("Arrested Cells" in Fig. 2) or released and fixed
554 12 hours post-release ("Cycling Cells" in Fig. 2).

555 **Immunofluorescence**

556 Immunofluorescence assays were performed as described previously (*29, 43*). NIH/3T3 and IMR-90
557 cells were fixed with 2% paraformaldehyde (PFA) (Electron Microscopy Sciences, cat# 15710) for 8
558 min at room temperature, washed 3 times with DPBS (Gibco, cat# 14190-136), and then permeabilized
559 with 0.25% Triton X-100 (ThermoFisher Scientific/Invitrogen, cat# 28314) for 10 min. Then, cells
560 were washed 3 times with DPBS for 5 min and blocked in 1% BSA (Sigma-Aldrich, cat# A4503) in
561 PBS-T (DPBS with 0.05% Tween 20, pH 7.4 (ThermoFisher Scientific/Invitrogen, cat# 28320)) for
562 60 min. Next, primary antibodies diluted in 1% BSA/TBS-T were added for 1 h, then samples were
563 washed three times with PBS-T for 5 min and incubated with secondary antibodies in 1% BSA/TBS-
564 T for 60 min followed by washing twice with PBS-T and one time with PBS for 5 min. Samples were
565 mounted using Duolink® In Situ Mounting Medium with DAPI (Sigma-Aldrich, cat# DUO82040-
566 5ML). All steps were performed at room temperature.

567 **Image acquisition and analysis**

568 All confocal immunofluorescent images were taken using a Leica SP8 laser scanning confocal system
569 using 63X/1.40 HC PL APO CS2 objective and HyD detectors in the standard mode with 100% gain.
570 3D images of the nuclei middle Z-planes were taken as Z-stacks with 0.1 μm intervals with a range of
571 1 μm per nucleus. Confocal 3D images were deconvoluted using Huygens Professional software by
572 utilizing the microscope parameters, standard PSF and automatic settings for background estimation.
573 Image analysis was performed using ImageJ software (National Institutes of Health, MD). The fraction
574 of the immunofluorescence signal at the nuclear lamina was determined as proportion of signal at the
575 nuclear lamina, measured using a mask of the nuclear lamina signal, to the total signal in the nucleus.
576 Analysis of PRR14 colocalization with heterochromatin was performed using Colocalization
577 Threshold tool in ImageJ with automatic parameters. Pearson's above threshold coefficient was
578 measured.

579 **Fluorescence recovery after photobleaching**

580 FRAP imaging was performed on a Leica SP8 laser scanning confocal system equipped with a
581 temperature control incubation chamber and an 63X/1.40 HC PL APO CS2 objective. NIH/3T3 cells
582 were plated on 8-well ibidi μ-slides and transfected with GFP-tagged human PRR14 constructs. FRAP
583 was performed 48 hours post-transfection using LAS X software (Leica Microsystems, Buffalo Grove,
584 IL) with a build-in FRAP wizard at 488 nm laser and a PMT detector. Live cells were imaged using a
585 1x Live Cell Imaging Solution (ThermoFisher Scientific/Invitrogen, cat# A14291DJ) and in a
586 temperature and humidity-controlled microscope chamber set at 37ºC. Briefly, a region of interest
587 (ROI) was bleached for about 4 seconds, then recovery of GFP-PRR14 signal was measured for 40-
588 120 seconds at 0.75-1.5s intervals. Fluorescence intensity of the bleached region of interest (ROI) and
589 total fluorescence intensity of the nucleus was measured using ImageJ software (National Institutes of
590 Health, MD). Out of focus frames were excluded from the analysis. To compensate for the inherent
591 baseline photobleaching over time, the overall recovery signal was normalized to the inherent
592 photobleaching rate of whole nucleus regions. Fluorescent recovery curve fitting and extension was
593 performed in GraphPad Prism 9 software (GraphPad Software, Inc.), as well as calculation of a
594 recovery half-time and an immobile fraction.

595 **Super-resolution microscopy**

596 Super-resolution imaging was performed using Stochastic Optical Reconstruction Microscopy
597 (STORM). Images were obtained using ONI Nanoimager (ONI Inc., CA). Cells were plated on 8-well
598 ibidi μ-slides and transfected with pCMV6-AN-mGFP-PRR14. Lamin A/C and H3K9me3 staining
599 was performed on untransfected cells. 48 hours post-transfection, samples were fixed, immunostained
600 as described above, and kept in DPBS until image acquisition. Secondary antibodies were conjugated
601 with Alexa 647 dye. Imaging acquisition was performed in fresh imaging buffer (50 mM Tris-HCl,
602 pH 8.0, 10 mM NaCl, 10% (w/v) glucose (Sigma-Aldrich, cat#G8270), 1.5 mg MEA (Sigma-Aldrich,
603 cat#30070), 170 AU Glucose oxidase (Sigma-Aldrich, cat#G2133), 1400 AU Catalase (Sigma-
604 Aldrich, cat#C40)). Images were processed using ONI Nanoimager™ Software version: 1.16 (ONI
605 Inc., CA).

606 **Immunoprecipitation experiments**

607 GFP-tagged PRR14 1-212 fragments (wild-type, site 1 mutant (54-55EE), site 2 mutant (154-155EE),
608 and DM (54-55EE and 154-155EE)) were transfected into Lenti-X 293T cells and used to assess
609 interactions with HP1 isoforms. Protein A/G Magnetic Beads (ThermoFisher Scientific, cat# 88802)
610 preincubated overnight at +4C° with anti-GFP antibodies or Normal Rabbit IgG were used for pull-
611 down of GFP-tagged proteins or as a mock pull-down. 48 hours post-transfection, cells were washed

612 in PBS, then scraped off the plates in 500 µL ice-cold NP-40 lysis buffer (VWR Life Science, cat#
613 J619-500ML) containing protease and phosphatase inhibitors (Roche, cat# 11697498001 and cat#
614 4906845001) and 1x benzonase (Sigma-Aldrich, cat# E1014-5KU). The lysates were then incubated
615 for 30 min at +4C° with constant agitation and cleared by centrifugation at 12,000 rpm for 20 min at
616 +4C°. The supernatants were collected and mixed with GFP antibody pre-conjugated beads, which
617 were pre-washed with NP-40 lysis buffer with protease/phosphatase inhibitors (Roche, cat#
618 11697498001 and cat# 4906845001) and incubated for 2.5 hours at +4C° with gentle agitation. The
619 beads were collected, washed with lysis buffer, resuspended in lysis buffer containing 1x NuPAGE
620 Sample Reducing Agent (ThermoFisher Scientific/Invitrogen, cat# NP0004), 1x Laemmli Sample
621 Buffer (Bio-Rad, cat# 1610747) and heated for 5 min at 95°C to dissociate immunocomplexes from
622 the beads. The beads were then cleared on a magnet, and the supernatants were collected. Proteins
623 were separated on 4-12% SDS–PAGE gels (ThermoFisher Scientific/Invitrogen, cat# NP0335) and
624 Western blotting of a 0.2 µm nitrocellulose membrane (ThermoFisher Scientific/Invitrogen, cat#
625 LC2000) was performed to detect GFP-PRR14 and HP1 isoforms by probing the membrane with the
626 corresponding antibodies. The membranes were developed using ECL Prime Western Blotting
627 Detection Reagents (Amersham/Cytiva cat #RPN2232). Image analysis was performed using ImageJ
628 Software. In brief, raw RGB Western Blot images were converted into 8-bit, and the colors were
629 inverted. Each band then was selected using an ImageJ Rectangular Tool, and the signal from the
630 selected areas was measured as a mean intensity value. The mean intensity value of the "double-mutant
631 DM" condition was then subtracted from the values measured for the rest of the experimental
632 conditions. Then, the values corresponding to HP1 proteins were normalized to the values of total IP:
633 GFP-PRR14 signal following with a second normalization to the maximum values within each
634 experimental condition.

635 **Antibodies**

636 The following primary antibodies were used in this study: anti-H3K9me3 (Abcam, cat# ab8898; IF
637 1:1000), anti-H3K9me2 (Active Motif, cat# 39239, IF 1:1000), anti-Lamin A/C (Santa Cruz, cat# sc-
638 376248; IF 1:500), anti-Lamin B1 (Abcam, cat# ab16048; IF 1:1000), anti-GFP (Abcam, cat# ab290;
639 WB 1:1000, IP 1:200), Normal Rabbit IgG (Cell Signaling, cat# 2729; IP 1:200), anti-HP1α (Abcam,
640 cat# 77256; IF, WB 1:1000), anti-HP1β (Abcam, cat# ab10478; IF, WB 1:1000), anti-HP1γ (Santa
641 Cruz, sc-398562; IF 1:500, WB 1:1000).

642 The following secondary antibodies from ThermoFisher Scientific/Invitrogen were used: Donkey anti-
643 Rabbit Alexa Fluor 568 (cat# A10042, IF 1:1000), Donkey anti-Mouse Alexa Fluor 488 (cat# A10037,
644 IF 1:1000), Donkey anti-Rabbit Alexa Fluor 647 (cat# A31573, IF 1:1000), Donkey anti-Mouse Alexa

645 Fluor 647 (cat# A31571, IF 1:1000); and HRP-linked anti-Rabbit IgG and HRP-linked anti-Mouse
646 IgG (Cell Signaling, cat# 7074 and 7076; WB 1:1000). IF – immunofluorescence, WB – Western Blot,
647 IP – immunoprecipitation.

648 **Statistical analysis**

649 For immunofluorescence assays, 10 to 40 individual cells were imaged per condition. These numbers
650 exceed the sample size calculated using power analysis. We considered each imaged individual
651 cell/nucleus as a biological replicate. The numbers of cells per each analysis are indicated in the figure
652 legends. Statistical analysis was performed with GraphPad Prism 9.3.1 software (GraphPad Software,
653 Inc.) using one-way Analysis of Variation (ANOVA) Brown-Forsythe and Welch test with Dunnett's
654 multiple comparisons (for samples with Gaussian distribution of residuals), paired ANOVA test with
655 Geisser-Greenhouse correction for immunoblot assay, or non-parametric ANOVA Kruskal-Wallis test
656 with Dunn's multiple comparison test. For comparison of two sample an unpaired non-parametric
657 Student's t-test (Mann–Whitney test) was used.

Author Contributions

Conceptualization: A.A.K., R.A.K. and A.P. Methodology: A.A.K., Y.C., C.L.S., and A.P. Formal analysis: A.A.K. and A.P. Investigation: A.A.K., Y.C., and A.P. Visualization: A.A.K. and A.P. Data curation: A.A.K. and A.P. Resources: R.A.K. Supervision: A.P. Writing (original draft): A.P. Writing (review and editing): A.A.K, R.A.K., C.L.S., and A.P.

Acknowledgments

We thank Jonathan A. Epstein for support (NIH R35 HL140018) and for discussions and comments on the manuscript. Rajan Jain for critical assessment of the manuscript and for helpful suggestions. Kelly Dunlevy, Jason Wasserman, Jade Wilson, Valentina Medvedeva, and Trinity Pellegrin for help with making certain constructs. Andrea Stout from the Penn CDB Microscopy Core for help with confocal imaging. Melike Lakadamyali for help with super-resolution imaging. Center for Engineering and Mechanobiology (CEMB) and NSF Science and Technology Center Pilot Award (CMMI 15-48571) for access to ONI super-resolution microscope. Penn Flow Cytometry Core for technical support.

Funding

This work was supported by the National Institutes of Health (NIH) (R35 HL140018 supported A.P. and C.L.S., R21 AG054829 to R.A.K., and P30 CA006927), American Heart Association (AHA) (827458 to A.A.K.).

Declaration of Interests

Authors declare no competing interests.

Data and materials availability

All data needed to evaluate the conclusions in the paper are present in the paper and/or the Supplementary Materials.

686

687 **REFERENCES**

688

689 1. A. Buchwalter, J. M. Kaneshiro, M. W. Hetzer, Coaching from the sidelines: the nuclear
690 periphery in genome regulation. *Nat Rev Genet* **20**, 39-50 (2019).
691 2. W. A. Bickmore, The spatial organization of the human genome. *Annu Rev Genomics Hum*
692 *Genet* **14**, 67-84 (2013).
693 3. G. Andrey, S. Mundlos, The three-dimensional genome: regulating gene expression during
694 pluripotency and development. *Development* **144**, 3646-3658 (2017).
695 4. M. Amendola, B. van Steensel, Mechanisms and dynamics of nuclear lamina-genome
696 interactions. *Curr Opin Cell Biol* **28**, 61-68 (2014).
697 5. D. Peric-Hupkes *et al.*, Molecular maps of the reorganization of genome-nuclear lamina
698 interactions during differentiation. *Mol Cell* **38**, 603-613 (2010).
699 6. L. Guelen *et al.*, Domain organization of human chromosomes revealed by mapping of nuclear
700 lamina interactions. *Nature* **453**, 948-951 (2008).
701 7. M. Bustin, T. Misteli, Nongenetic functions of the genome. *Science* **352**, aad6933 (2016).
702 8. I. Solovei *et al.*, Nuclear architecture of rod photoreceptor cells adapts to vision in mammalian
703 evolution. *Cell* **137**, 356-368 (2009).
704 9. I. Guerreiro, J. Kind, Spatial chromatin organization and gene regulation at the nuclear lamina.
705 *Curr Opin Genet Dev* **55**, 19-25 (2019).
706 10. A. Gonzalez-Sandoval, S. M. Gasser, On TADs and LADs: Spatial Control Over Gene Expression.
707 *Trends Genet* **32**, 485-495 (2016).
708 11. J. Kind, B. van Steensel, Genome-nuclear lamina interactions and gene regulation. *Curr Opin*
709 *Cell Biol* **22**, 320-325 (2010).
710 12. A. Poleshko *et al.*, Genome-Nuclear Lamina Interactions Regulate Cardiac Stem Cell Lineage
711 Restriction. *Cell* **171**, 573-587 e514 (2017).
712 13. A. Gonzalez-Sandoval *et al.*, Perinuclear Anchoring of H3K9-Methylated Chromatin Stabilizes
713 Induced Cell Fate in C. elegans Embryos. *Cell* **163**, 1333-1347 (2015).
714 14. P. P. Shah *et al.*, Pathogenic LMNA variants disrupt cardiac lamina-chromatin interactions and
715 de-repress alternative fate genes. *Cell Stem Cell* **28**, 938-954 e939 (2021).
716 15. S. G. Manzo, L. Dauban, B. van Steensel, Lamina-associated domains: Tethers and looseners.
717 *Curr Opin Cell Biol* **74**, 80-87 (2022).
718 16. D. Makatsori *et al.*, The inner nuclear membrane protein lamin B receptor forms distinct
719 microdomains and links epigenetically marked chromatin to the nuclear envelope. *J. Biol.*
720 *Chem.* **279**, 25567-25573 (2004).
721 17. M. S. Lechner, D. C. Schultz, D. Negorev, G. G. Maul, F. J. Rauscher, 3rd, The mammalian
722 heterochromatin protein 1 binds diverse nuclear proteins through a common motif that
723 targets the chromoshadow domain. *Biochem. Biophys. Res. Commun.* **331**, 929-937 (2005).
724 18. A. Poleshko *et al.*, The human protein PRR14 tethers heterochromatin to the nuclear lamina
725 during interphase and mitotic exit. *Cell Rep.* **5**, 292-301 (2013).
726 19. E. Minc, Y. Allory, H. J. Worman, J. C. Courvalin, B. Buendia, Localization and phosphorylation
727 of HP1 proteins during the cell cycle in mammalian cells. *Chromosoma* **108**, 220-234 (1999).
728 20. D. O. Jones, I. G. Cowell, P. B. Singh, Mammalian chromodomain proteins: their role in
729 genome organisation and expression. *Bioessays* **22**, 124-137 (2000).

730 21. L. Bosch-Presegue *et al.*, Mammalian HP1 Isoforms Have Specific Roles in Heterochromatin
731 Structure and Organization. *Cell Rep* **21**, 2048-2057 (2017).
732 22. A. Kumar, H. Kono, Heterochromatin protein 1 (HP1): interactions with itself and chromatin
733 components. *Biophys Rev* **12**, 387-400 (2020).
734 23. C. Maison, G. Almouzni, HP1 and the dynamics of heterochromatin maintenance. *Nat Rev*
735 *Mol Cell Biol* **5**, 296-304 (2004).
736 24. E. Minc, J. C. Courvalin, B. Buendia, HP1gamma associates with euchromatin and
737 heterochromatin in mammalian nuclei and chromosomes. *Cytogenet Cell Genet* **90**, 279-284
738 (2000).
739 25. A. L. Nielsen *et al.*, Heterochromatin formation in mammalian cells: interaction between
740 histones and HP1 proteins. *Mol Cell* **7**, 729-739 (2001).
741 26. G. Lomberk, L. Wallrath, R. Urrutia, The heterochromatin protein 1 family. *Genome Biol.* **7**,
742 228 (2006).
743 27. M. Lachner, D. O'Carroll, S. Rea, K. Mechtler, T. Jenuwein, Methylation of histone H3 lysine 9
744 creates a binding site for HP1 proteins. *Nature* **410**, 116-120 (2001).
745 28. A. L. Olins, G. Rhodes, D. B. Welch, M. Zwerger, D. E. Olins, Lamin B receptor: multi-tasking at
746 the nuclear envelope. *Nucleus* **1**, 53-70 (2010).
747 29. K. L. Dunlevy *et al.*, The PRR14 heterochromatin tether encodes modular domains that
748 mediate and regulate nuclear lamina targeting. *J Cell Sci* **133**, (2020).
749 30. A. Poleshko *et al.*, Human factors and pathways essential for mediating epigenetic gene
750 silencing. *Epigenetics* **9**, 1280-1289 (2014).
751 31. A. Poleshko, R. A. Katz, Specifying peripheral heterochromatin during nuclear lamina
752 reassembly. *Nucleus* **5**, 32-39 (2014).
753 32. C. L. Smith, Y. Lan, R. Jain, J. A. Epstein, A. Poleshko, Global chromatin relabeling accompanies
754 spatial inversion of chromatin in rod photoreceptors. *Sci Adv* **7**, eabj3035 (2021).
755 33. A. Vertii *et al.*, Two contrasting classes of nucleolus-associated domains in mouse fibroblast
756 heterochromatin. *Genome Res* **29**, 1235-1249 (2019).
757 34. M. Guenatri, D. Bailly, C. Maison, G. Almouzni, Mouse centric and pericentric satellite repeats
758 form distinct functional heterochromatin. *J Cell Biol* **166**, 493-505 (2004).
759 35. R. D. Goldman, Y. Gruenbaum, R. D. Moir, D. K. Shumaker, T. P. Spann, Nuclear lamins:
760 building blocks of nuclear architecture. *Genes Dev* **16**, 533-547 (2002).
761 36. M. S. Lechner, D. C. Schultz, D. Negorev, G. G. Maul, F. J. Rauscher, 3rd, The mammalian
762 heterochromatin protein 1 binds diverse nuclear proteins through a common motif that
763 targets the chromoshadow domain. *Biochem Biophys Res Commun* **331**, 929-937 (2005).
764 37. S. Machida *et al.*, Structural Basis of Heterochromatin Formation by Human HP1. *Mol Cell* **69**,
765 385-397 e388 (2018).
766 38. K. Romeo *et al.*, The SENP7 SUMO-Protease Presents a Module of Two HP1 Interaction Motifs
767 that Locks HP1 Protein at Pericentric Heterochromatin. *Cell Rep* **10**, 771-782 (2015).
768 39. M. Yang, Z. M. Yuan, A novel role of PRR14 in the regulation of skeletal myogenesis. *Cell Death*
769 *Dis* **6**, e1734 (2015).
770 40. D. H. Lee, H. W. Ryu, G. W. Kim, S. H. Kwon, Comparison of three heterochromatin protein 1
771 homologs in Drosophila. *J Cell Sci* **132**, (2019).
772 41. D. Canzio, A. Larson, G. J. Narlikar, Mechanisms of functional promiscuity by HP1 proteins.
773 *Trends Cell Biol* **24**, 377-386 (2014).
774 42. M. Yang, M. Lewinska, X. Fan, J. Zhu, Z. M. Yuan, PRR14 is a novel activator of the PI3K
775 pathway promoting lung carcinogenesis. *Oncogene* **35**, 5527-5538 (2016).

776 43. A. Poleshko *et al.*, H3K9me2 orchestrates inheritance of spatial positioning of peripheral
777 heterochromatin through mitosis. *Elife* **8**, (2019).
778 44. J. Kind *et al.*, Single-cell dynamics of genome-nuclear lamina interactions. *Cell* **153**, 178-192
779 (2013).
780 45. G. Chen, X. Deng, Cell Synchronization by Double Thymidine Block. *Bio Protoc* **8**, (2018).
781

Supplementary Materials for

PRR14 organizes H3K9me3-modified heterochromatin at the nuclear lamina

Anna A. Kiseleva, Yu-Chia Cheng, Richard A. Katz, Cheryl L. Smith, Andrey Poleshko*

*Corresponding authors. Email: poleshko@pennmedicine.upenn.edu

Supplementary file includes:

Figs. S1 to S9

Source data includes:

Raw Western blot images for Figure 5 and Figure S5.

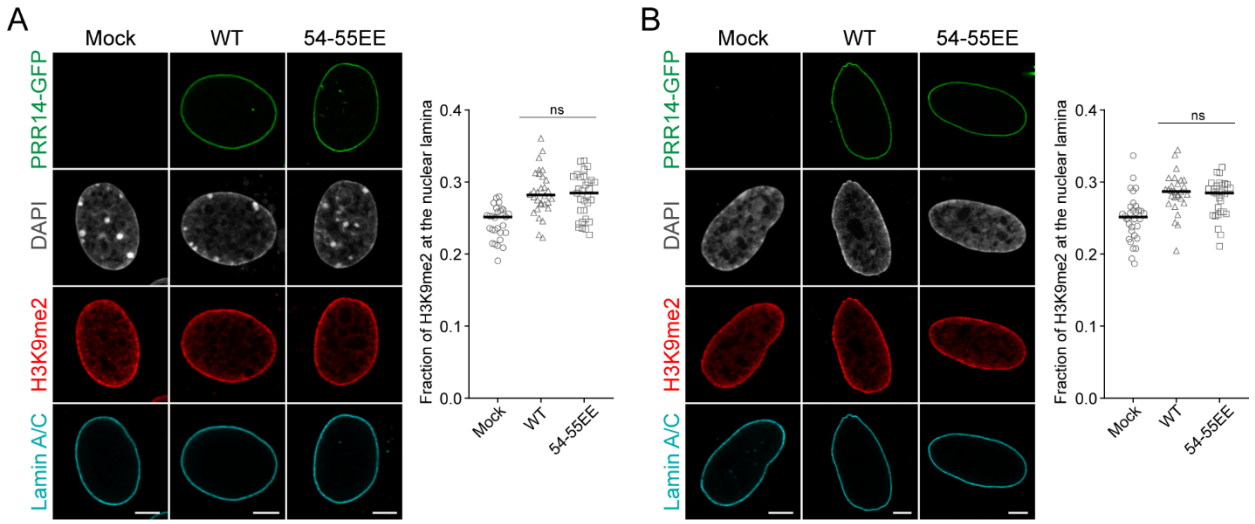

Figure S1. PRR14 overexpression shows no significant effect on H3K9me2-modified heterochromatin localization at the nuclear lamina. Representative confocal images of **(A)** murine NIH/3T3 and **(B)** human IMR-90 cells expressing WT or 54-55EE mutant GFP-tagged PRR14 constructs (green), stained for H3K9me2 (red) and Lamin A/C (cyan). DAPI counterstain shown in gray. Dot plots show the fraction of H3K9me2 signal at the nuclear lamina. n ≥ 30 cells per condition. Lines on dot plots show median values. Statistical analysis was performed using ANOVA Kruskal-Wallis test with Dunn's multiple comparisons; ns: not significant. Scale bars 5μm.

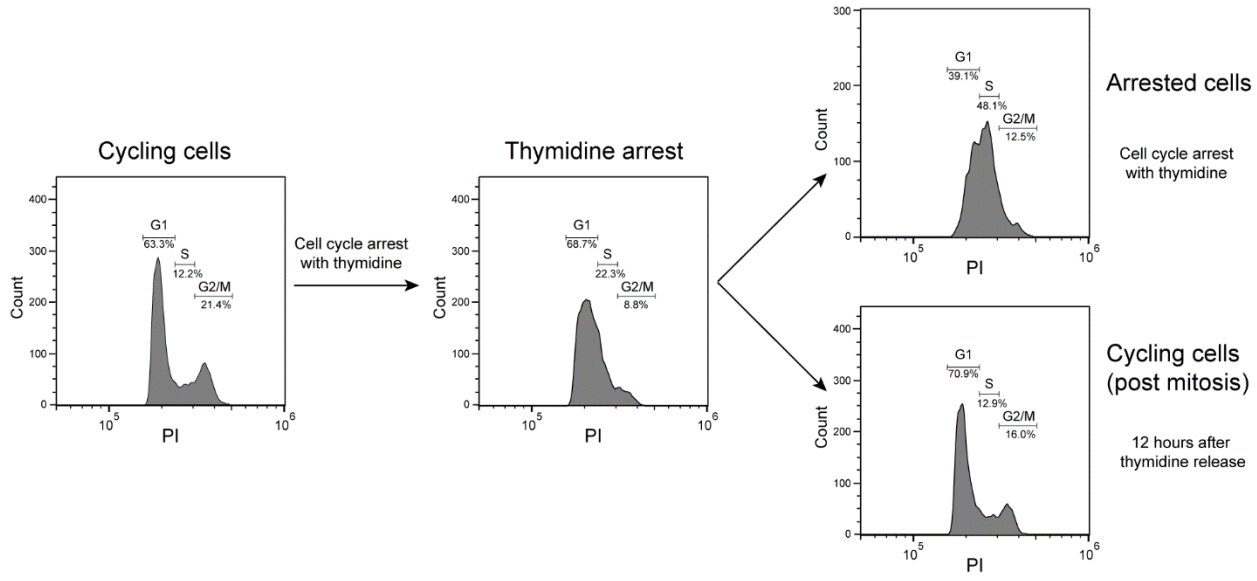

Figure S2. Flow cytometry charts of cell-cycle arrest with thymidine. NIH/3T3 cells transfected with PRR14-GFP were arrested with thymidine to prevent mitosis. Samples were maintained in thymidine to prevent mitosis or released from thymidine block 12 hours before fixation to allow mitosis. Flow cytometry charts show normal cycling cells, thymidine-arrested cells, arrested cells 12 hours post-thymidine treatment, and post-mitotic cells 12 hours after thymidine release. G1, S, and G2/M gates show percentage of cells in indicated cell-cycle stages. PI, propidium iodide.

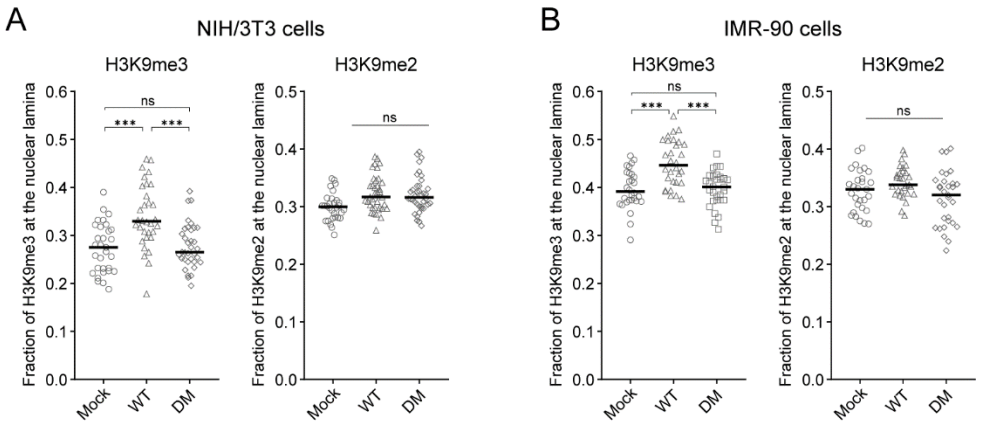

Figure S3. PRR14 specifically organizes H3K9me3-modified but not H3K9me2-modified chromatin at the nuclear periphery. To exclude the possibility that PRR14 HP1-binding site 2 (LVVML) functions to bind and tether H3K9me2, we performed the same experiment as in Figure 1 and Figure S1 with PRR14 double mutant (DM) construct (54-55EE and 154-155EE). We observed no differences compare to results presented in Figure 1 or Figure S1. Dot plots show fractions of H3K9me2- and H3K9me3-marked chromatin at the nuclear lamina in **(A)** NIH/3T3 and (**B**) IMR-90 cells transfected with WT or DM PRR14. n > 35 cells per condition. Statistical analysis was performed using ANOVA Kruskal-Wallis test with Dunn's multiple comparisons; ***p < 0.001, ns: not significant.

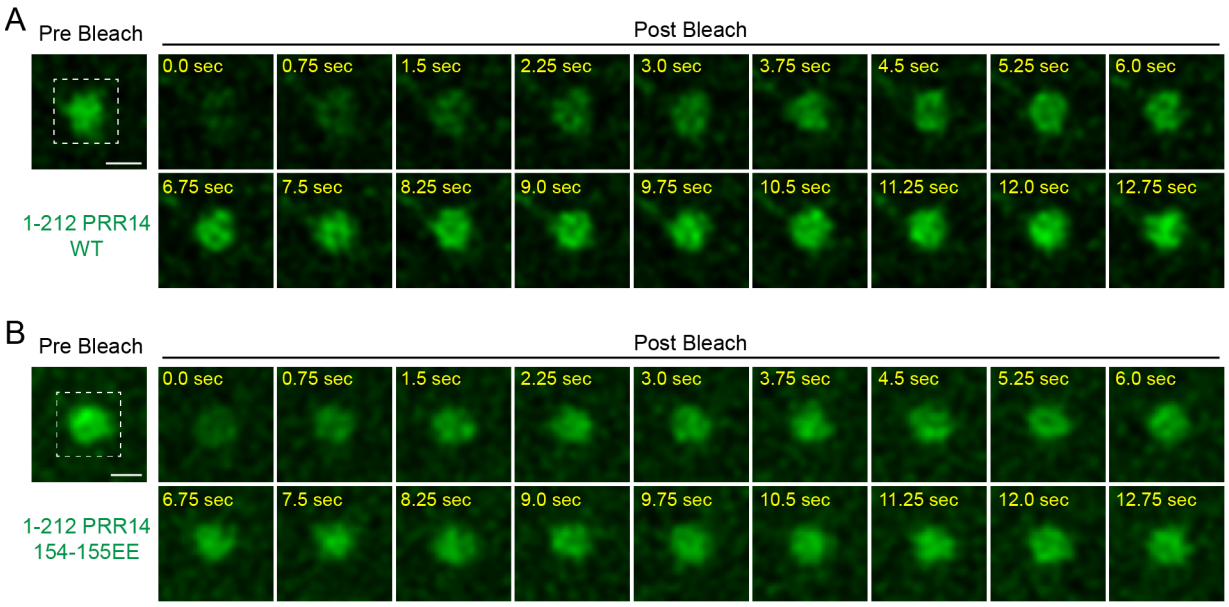

Figure S4. PRR14 association with the nuclear lamina is independent of PRR14-heterochromatin binding. Zoomed regions of representative confocal images shown in Figure 4 of fluorescence recovery after photobleaching (FRAP) assay of WT 1-212 PRR14 and mutant construct 154-155EE. Scale bars 1μm.

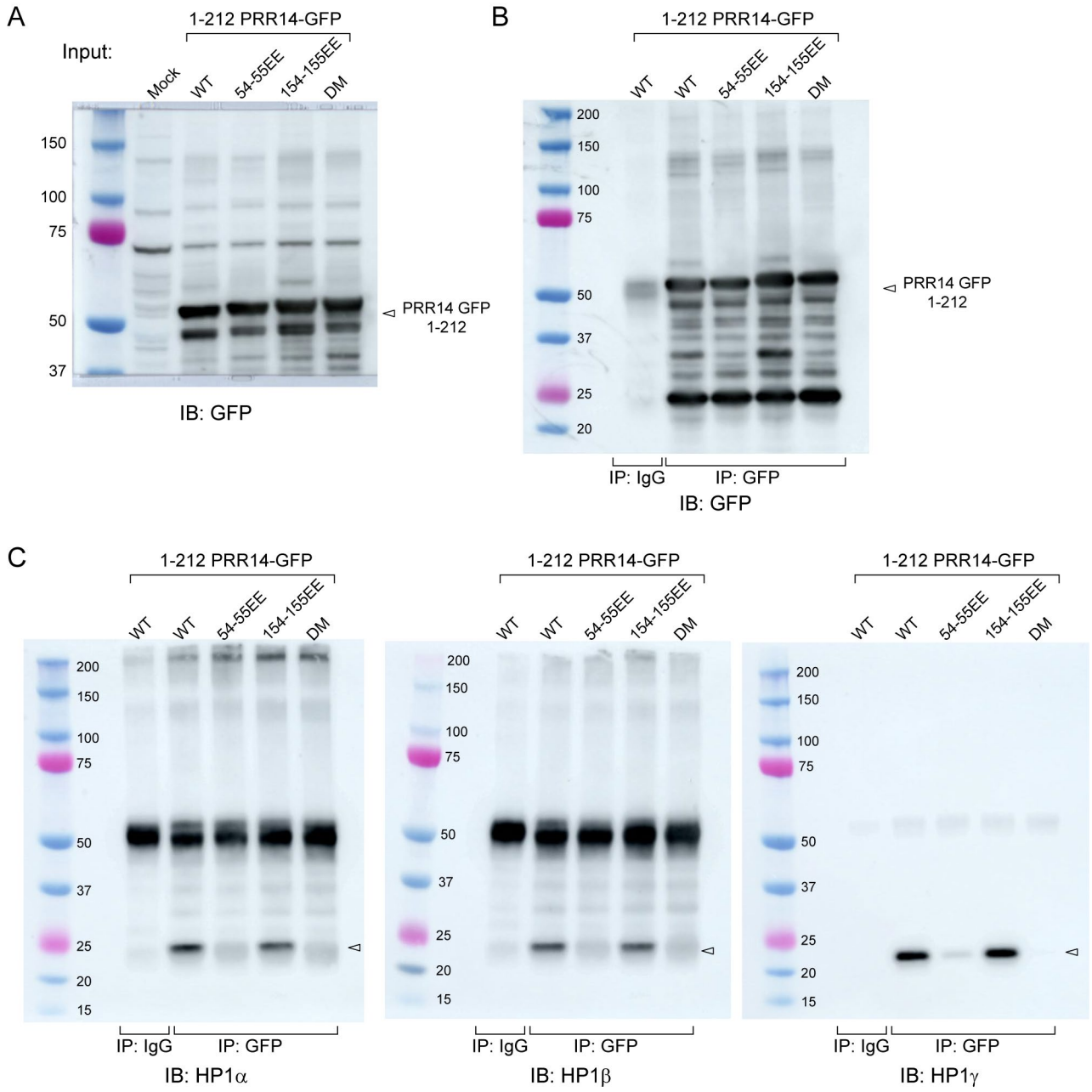

Figure S5. Representative images of Western blot experiments. (A) Immuno-blot (IB) shows sample inputs for immunoprecipitation followed by HP1 isoform Western blot experiment with overexpressed GFP-PRR14 1-212 fragment (WT or mutants as indicated). The membrane was immuno-blotted with anti-GFP antibodies. **(B)** Immunoprecipitation (IP) of indicated samples with anti-IgG or anti-GFP antibody, immuno-blotted with anti-GFP antibody. **(C)** Immunoprecipitation (IP) of indicated samples with anti-IgG or anti-GFP antibody, immuno-blotted (IB) with anti-HP1α (left), anti-HP1β (middle) and anti-HP1γ (right) antibodies. Arrowheads show HP1 protein bands.

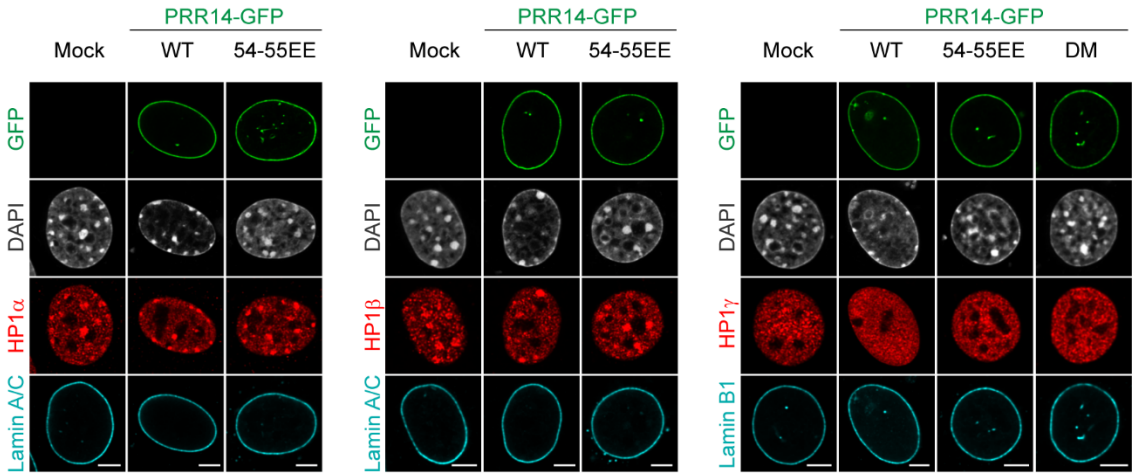

Figure S6. Overexpression of PRR14 results in repositioning of HP1 proteins towards the nuclear periphery. Representative confocal images show expression of WT PRR14-GFP or mutant forms and localization of HP1α, HP1β, and HP1γ (in red) in NIH/3T3 nuclei. Scale bars 5μm.

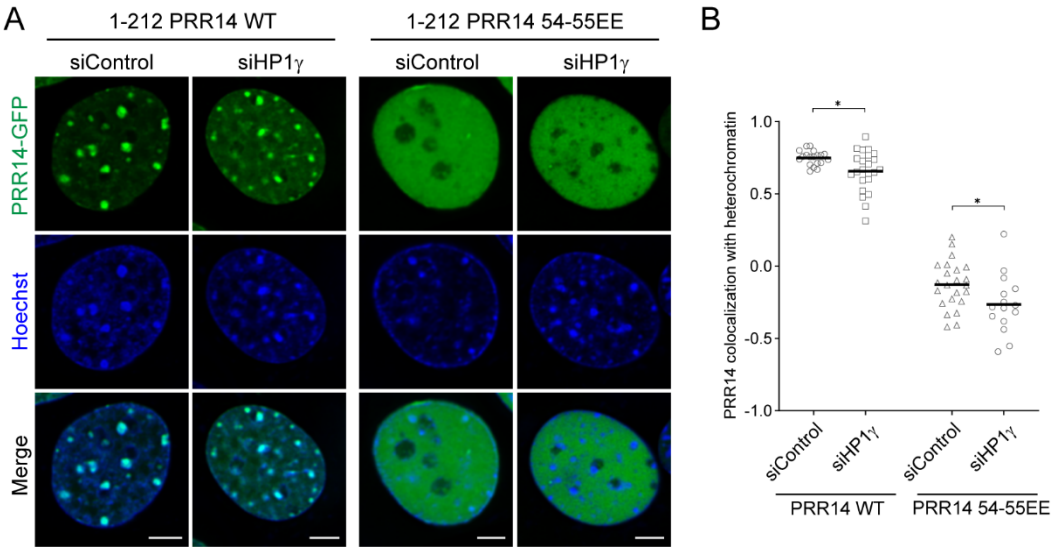

Figure S7. Knockdown of HP1γ decreases PRR14 efficiency for chromatin binding. (A) Representative confocal images of murine NIH/3T3 cells expressing indicated WT or mutant GFP-tagged 1-212 PRR14 constructs (green), counterstained with Hoechst (blue). **(B)** Dot plot shows the Pearson's correlation of Hoechst staining and GFP-PRR14 signal for each PRR14 construct indicating degree of colocalization of PRR14 with heterochromatin regions. n ≥ 15 cells per condition. Lines on the dot plot show median values. Statistical analysis was performed using Mann-Whitney test; *$p < 0.05$. Scale bars 5μm.

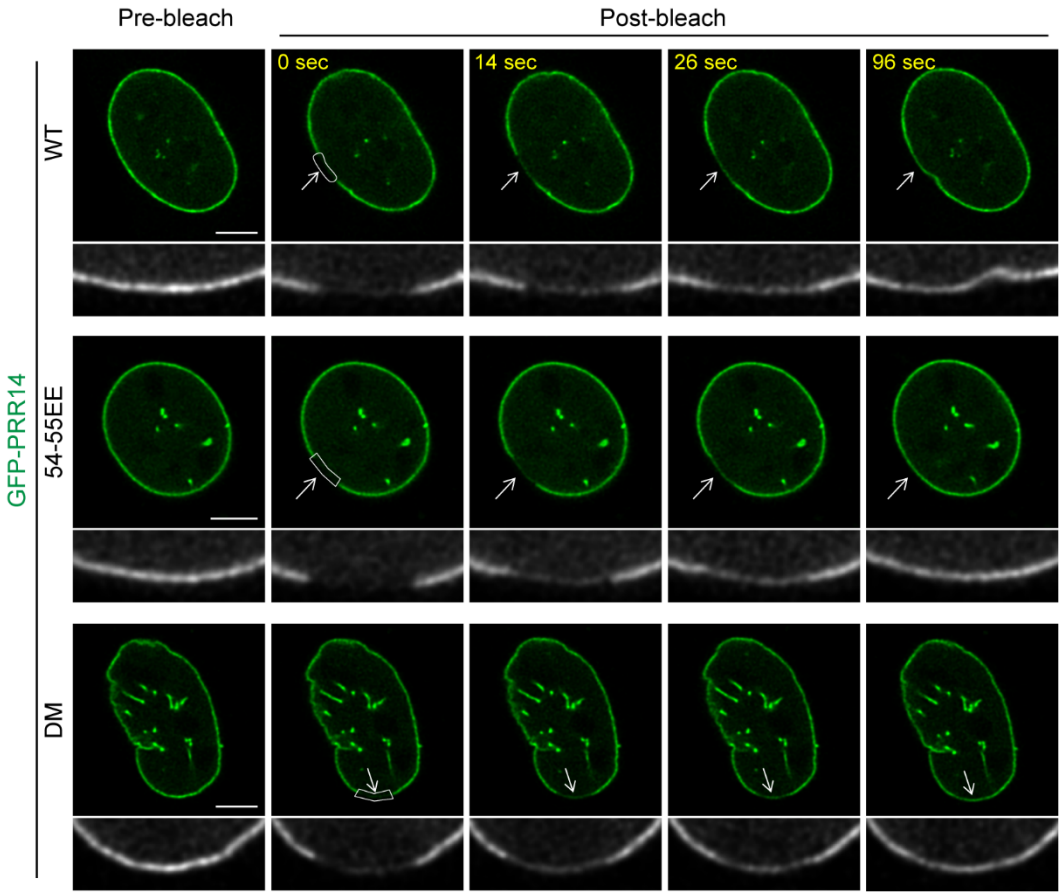

Figure S8. PRR14 association with the nuclear lamina is independent of PRR14-heterochromatin binding. Representative confocal images of fluorescence recovery after photobleaching (FRAP) assay of WT full-length PRR14-GFP and mutant constructs in NIH/3T3 cells. DM, double mutant (54-55EE and 154-155EE). Scale bars 5μm.

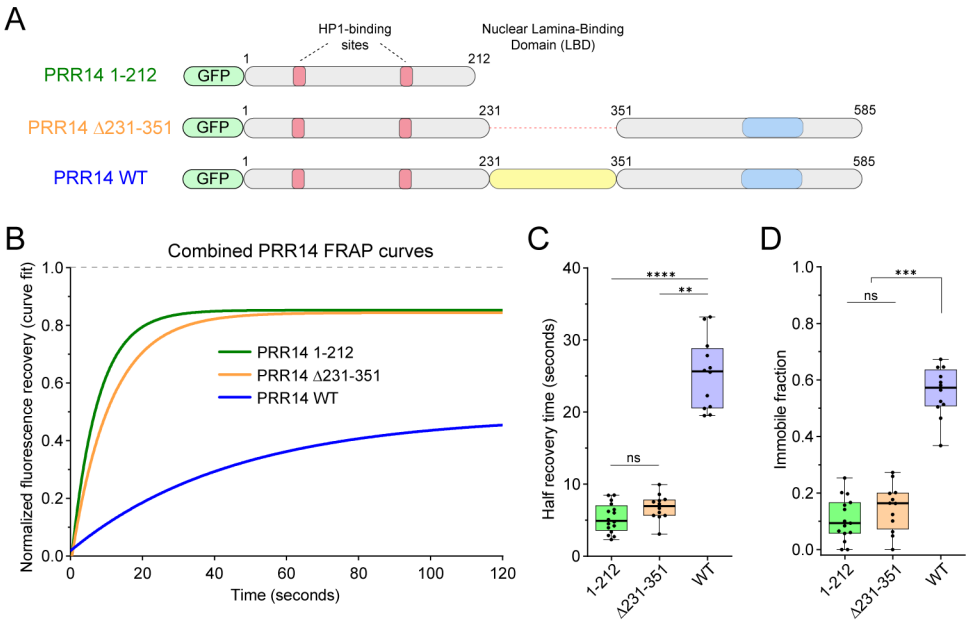

Figure S9. PRR14 shows rapid exchange with heterochromatin, compared to less dynamic full-length WT PRR14 association with the nuclear lamina. To determine whether the rapid PRR14 dynamics of interaction with heterochromatin result from the smaller size of the GFP-PRR14 1-212 fragment (450 aa) used in the FRAP assay compared to the full-length PRR14 (823 aa), we performed a FRAP assay with a GFP-PRR14 construct that carries a deletion of LBD (PRR14 Δ231-351) which is close in size (703 aa) to the full-length protein. We demonstrated that both PRR14 1-212 and Δ213-351 fragments that lack interaction with the nuclear lamina, show similar dynamics with minor differences compared to full-length PRR14 protein. **(A)** Schematic representation of PRR14 fragments including only heterochromatin-binding domain (PRR14 1-212), a fragment with deletion of the lamina-binding domain (PRR14 Δ231-351), and full-length wild-type protein (PRR14 WT). **(B)** Line graph shows extended curve fits of normalized fluorescent recovery over time after photobleaching of indicated PRR14 constructs. **(C)** Box plot shows distributions of recovery half-times for indicated PRR14 constructs. **(D)** Box plot shows distributions of immobile fractions for indicated constructs. n ≥ 12 cells per condition. Box plots show median, 25th and 75th percentiles. Whiskers show minimum to maximum range. Statistical analysis was performed using ANOVA Kruskal-Wallis test with Dunn's multiple comparisons. ****$p < 0.0001$, ***$p < 0.001$, **$p < 0.01$, ns: not significant.